39

Nanocomposite Catalysts for Steam Reforming of Methane and Biofuels: Design and Performance

Vladislav Sadykov, Natalia Mezentseva, Galina Alikina, Rimma Bunina, Vladimir Pelipenko, Anton Lukashevich, Zakhar Vostrikov, Vladimir Rogov, Tamara Krieger, Arkady Ishchenko, Vladimir Zaikovsky, Lyudmila Bobrova, Julian Ross, Oleg Smorygo, Alevtina Smirnova, Bert Rietveld and Frans van Berkel,
[1]*Boreskov Institute of Catalysis, Novosibirsk State University*,
[2]*University of Limerick*,
[3]*Powder Metallurgy Institute*,
[4]*Eastern Connecticut State University*,
[5]*Energy Research Center of the Netherlands*,
[1]*Russia*
[2]*Ireland*
[3]*Belarus*
[4]*USA*
[5]*Netherlands*

1. Introduction

Design of nanocomposite materials with high mixed ionic-electronic conductivity (MIEC) and oxygen mobility possessing a high and stable performance in real operation conditions is now considered as one of the most promising trend in developing new anode materials for IT SOFC (Primdahl & Mogensen, 2002; Atkinson et al., 2004; Wincewicz & Cooper, 2005; Dicks, 1998; Kharton et al, 2006; Marina et al, 1999; Xia & Liu, 2002; Zha et al, 2004; Ishihara et al, 2000) and structured catalysts for steam/autothermal reforming of gas and liquid fuels (Souza & Schmal, 2003; Domine et al., 2008; Sadykov et al., 2009).

State-of-the art Ni/Y_2O_3–ZrO_2 (Ni/YSZ) cermet anodes of solid oxide fuel cells (SOFC) have excellent catalytic properties and stability in the oxidation of hydrogen fuel at SOFC operation conditions (Atkinson et al., 2004). However, the lack of a hydrogen infrastructure and the unsolved hydrogen storage problem have initiated the research aimed at direct utilization of natural gas, which represents one of the key aspects of SOFC technology. Internal steam reforming (SR) is the most promising concept in using the natural gas (as well as bio-gas or bioethanol) as a fuel (Wincewicz & Cooper, 2005; Dicks, 1998). In this case, the reaction takes place directly in the anode compartment, allowing a better management within the stack of heat produced by the exothermic electrochemical oxidation and consumed by the endothermic reforming reaction. Unfortunately, with the Ni/YSZ cermet,

coking occurs leading to the deterioration of anode performance (Atkinson et al., 2004; Dicks, 1998). Under high carbon activity environment, Ni metal could also be corroded by the metal dusting. Ni/YSZ cermet anodes can only be used in hydrocarbon fuels if excess steam is present to suppress the carbon deposition, which, however, decreases the electrical efficiency of the cells (Wincewicz & Cooper, 2005; Dicks, 1998). Hence, development of robust anodes with a high and stable activity in the internal reforming of fuels is vital for the natural gas/biogas/bioethanol fuel-based SOFC. Next approaches were suggested up to date to solve this problem:

1. Partial or complete replacement of doped zirconia with doped ceria or ceria-zirconia possessing a higher lattice oxygen mobility/reactivity (Atkinson et al., 2004; Wincewicz & Cooper, 2005; Dicks, 1998; Kharton et al, 2006; Marina et al, 1999; Xia & Liu, 2002; Zha et al, 2004; Ishihara et al, 2000). This is combined with partial or complete replacement of Ni by copper (Dongare et al., 2002; Ana et al., 2004). This approach allows not only to prevent coking but also ensures a high performance in SR at intermediate temperatures. In this case, some problems could be caused by considerable chemical expansion of ceria lattice in strongly reducing conditions as well as by copper sintering.
2. Replacing doped zirconia by perovskites (mainly, doped La chromites) promoted by metals active in SR (Ni or precious metals, mainly, Ru) (Peña-Martínez et al., 2006; Sfeir et al., 2001; Sauvet & Irvine, 2004; Vernoux et al., 1998; Wan & Goodenough, 2005). In this case, insufficient conductivity of perovskites in reducing conditions could be a problem (Plint et al., 2006).
3. Partial or complete replacement of Ni in Ni/YSZ or Ni/perovskite cermets by precious metals (Wan & Goodenough, 2005; Bebelis et al., 2006; Suzuki et al., 1993; Takeguchi et al., 2003). This allows to suppress coking and enhance the middle-temperature performance which is explained by a much higher specific catalytic activity of precious metals in CH_4 SR, Pt being the most active metal (Wei & Iglesia, 2004). In the case of cermets containing only precious metals, apparent drawback is their high cost.

Hence, the most promising approach for achieving a high level of anode activity at middle temperatures in CH_4 steam reforming while preventing coking, keeping a high level of conductivity and a low cost, is to promote Ni/YSZ(ScSZ) cermets by fluorite-like (doped ceria-zirconia) or perovskite-like (mixed chromates-manganites) oxides along with small (~1%) amounts of precious metals (Pt, Pd, Ru). These (nano)composites are comprised of components able to efficiently activate C-H and C-C bonds in the fuel molecules (Ni, precious metals) and oxide components providing activation of water molecules and transfer of hydroxyls and/or hydroxocarbonate/oxygen species to the metal particles where they interact with activated C-H-O species producing syngas (Souza & Schmal, 2003).

In the last years biomass has been recognized as one of the major world renewable energy sources. Bio-oil derived from the fast pyrolysis of biomass or bio-ethanol can be converted via steam reforming into hydrogen or syngas, which can be further used in fuel cells or directed to synthesis of liquid fuels and valuable chemicals (Asadullah et al., 2002). For SOFC, an attractive option is direct internal reforming of bio-fuels on catalytically active anodes (Jamsak et al., 2007). Hence, efficient, inexpensive and robust catalysts for the steam reforming of biofuel are required. The most demanding problem of their design is a heavy coking of catalysts even in the feeds with the excess of steam caused by a high reactivity of bio-fuel components (carboxylic acids, aldehydes, ketones, alcohols etc), thus excluding application of traditional Ni-based steam reforming catalysts, Ni- YSZ anode cermets (Jamsak et al., 2007) or precious metals (Pt, Pd, Ru) supported on alumina, zirconia, etc

(Haryanto et al., 2005; Breen et al., 2002). Hence, inexpensive nanocomposite catalysts on the base of promoted Ni/could be also attractive as active and stable to coking components of catalysts for steam reforming of biofuels.

To ensure a high performance of these composites in steam reforming of a given type of fuel, their composition and preparation procedures are to be properly optimized. Specificity of functional characteristics of nanocomposite materials strongly depends on the properties of interfaces/domain boundaries which could act as paths for fast oxygen diffusion and generate specific surface sites responsible for activation of reagents. Chemical composition and local structure of these interfaces controlling their properties are determined both by the nature of coexisting phases and their interaction depending upon the size of domains, their disordering and nanocomposite synthesis procedure.

This chapter overviews results of research within the frames of a broad international collaboration supported by projects of INTAS, NATO Science for Peace and 6 EC Framework Program aimed at design of nanocomposite active components of catalysts for steam reforming of methane and biofuels into syngas both for the fuel cell application and synfuels production mainly published in last 5 years (Pavlova et al., 2007; Mezentseva et al., 2010; Sadykov et al., 2006c; 2008a,b; 2009a,b,c; 2010a,c; Yaseneva et al., 2008; 29-39). A lot of attention was paid to systematic studies of the effect of chemical composition of doped ceria-zirconia solid solutions on the real structure, oxygen mobility and reactivity in nanocomposites considered to be the most important factors controlling their performance. Information on the basic structural features and oxygen mobility/reactivity in Pt-supported ceria-zirconia solid solutions as well as their catalytic properties in transformation of methane and oxygenates into syngas studied earlier in details (Frolova et al., 2006; Sadovskaya et al, 2007; Sadykov et al., 2006b, 2007a-e, 2009a,d, 2010c) provide required bases for understanding the catalytic properties of nanocomposites containing these constituents.

Nanocomposites possessing promising performance and coking stability in target reactions were supported on anode substrates or heat-conducting metal substrates and successfully tested in realistic conditions in the in-cell methane steam reforming as well as in pilot -scale reactors of CH_4 or oxygenates transformation into syngas.

2. Real structure of (nano)composite materials: Effect of method of preparation on morphology and interaction between phases of composite

To provide compatibility of (nano)composites supported as porous layers on traditional Ni/YSZ cermet anodes (high ionic and electronic conductivity, close values of thermal and chemical expansion coefficients are required), the content of NiO and YSZ in composites is to be rather high. For nanocomposites supported as porous layers on heat-conducting substrates (Crofer interconnects, Ni-Al compressed foam substrates, Fechraloy foils/gauzes covered by protective corundum layer (Sadykov et al., 2008a, 2009c; 2010a), these restrictions are less severe, and the content of NiO and YSZ could be broadly varied as dependent upon the target application.

Hence, next types of (nano)composites were prepared and studied within this research program:

1. Composite **I** (specific surface area 11 m^2/g) comprised of 60 wt.% NiO+40 wt.% YSZ was prepared by mixing and ball milling of industrial sources followed by calcination at 900 ^oC for 2 h (Sadykov et al., 2008b). This composite containing rather big particles of NiO and YSZ was promoted by supporting 10 wt.% of fluorite-like ($Ce_{0.5}Zr_{0.5}O_{2-x}$,

$Pr_{0.3}Ce_{0.35}Zr_{0.35}O_2$, $La_{0.3}Ce_{0.35}Zr_{0.35}O_2$) or perovskite-like ($La_{0.8}Pr_{0.2}Mn_{0.2}Cr_{0.8}O_3$) oxides by impregnation with water solutions of corresponding polyester citric acid-ethylene glycol precursors followed by drying and calcination in air at 700 °C for 4 h.

2. Composite **II** (specific surface area 23 m^2/g) comprised of 10 wt.% $La_{0.8}Pr_{0.2}Mn_{0.2}Cr_{0.8}O_3$+55 wt.% NiO+35 wt.% ScCeSZ was prepared using powdered $Sc_{0.1}Ce_{0.01}Zr_{0.89}O_{2-y}$ electrolyte synthesized by co-precipitation as described elsewhere (Smirnova et al., 2007). ScCeSZ powder was first dispersed in the water solution of Ni nitrate and polyester citric acid-ethylene glycol polymeric precursor of perovskite following so called one-pot synthesis routine (Sadykov et al., 2005b). After evaporation, formed solid residue was decomposed in air at 500°C and then calcined at 700°C for 4 h.
3. Composite **III** (specific surface area 9 m^2/g) comprised of 60 wt.% NiO+40 wt.% YSZ was prepared by impregnation of powdered $Y_{0.08}Zr_{0.92}O_{2-y}$ (Russian source) with an excess of Ni nitrate solution followed by drying overnight in air at 90°C with subsequent calcination at 800°C. After regrinding, the composite **III** was loaded with 10 wt.% fluorite-like oxides ($Pr_xCe_yZr_zO_2$, $La_qPr_xCe_yZr_zO_2$, $Sm_qPr_xCe_yZr_zO_2$, where y = 0.35, 05; z = 0.35, 0.25, 0.2; x = 0.15-0.3; q = 0.15) by impregnation with respective mixed nitrates solutions followed by drying and calcination at 800 °C (Sadykov et al., 2009b).
4. Composite **IV** (specific surface area 28 m^2/g) comprised of 10 wt.% $Pr_{0.15}La_{0.15}Ce_{0.35}Zr_{0.35}O_2$+55 wt.% NiO+35 wt.% YSZ (Russian source) was prepared by the one-pot Pechini procedure similar to that used for preparation of composite **II**.
5. Composites of series **V** comprised of 10-80% $La_{0.8}Pr_{0.2}Mn_{0.2}Cr_{0.8}O_3$+ 90-20% (NiO + YSZ) were prepared by the one-pot Pechini procedure similar to that used for preparation of composite **II** [38]
6. Composites of series **VI** comprised of 10-80% $Sm_{0.15}Pr_{0.15}Ce_{0.35}Zr_{0.35}O_2$ + 90-20% (NiO + YSZ) were prepared by the one-pot Pechini procedure similar to that used for preparation of composite **II**.
7. Composites of series **VII** comprised of 80%$Pr_{0.30-x}Sm_xCe_{0.35}Zr_{0.35}O_2$ (x=0, 0.15, 0.3) +10%NiO + 10% $Y_{0.08}Zr_{0.92}O_{2-x}$ were prepared by the one-pot Pechini procedure similar to that used for preparation of composite **II**.

Pd, Pt, Ru or Pt + Ru (0.3-1.4 wt.%) were supported on composites by the incipient wetness impregnation with $PdCl_2$, H_2PtCl_6 or $RuCl_3$ solutions followed by drying and calcinations at 800°C for 2h.

2.1 Microstructural features of (nano)composites by TEM with EDX

2.1.1 Composites with a high content of NiO and YSZ

The initial composite I is comprised of bulky NiO particles and 8YSZ aggregates with a rather good crystallinity without any apparent interaction between these oxide phases (Fig. 1). The perovskite and fluorite phases present on the NiO surface generate a moiré pattern caused by overlapping of complex oxides and NiO lattices (Fig. 2). This suggests rather good epitaxy between these phases due to a strong chemical interaction.

Composite II (Fig. 3) is comprised of loose micron-size aggregates of nanoparticles with pronounced spatial variation of their composition as revealed by EDX. In this system, particles of NiO and perovskite-like phase possessing rather good crystallinity are stacked nearly coherently. In Fig. 4, the interphase boundary a–c corresponds to the ideally matched (100) $LnCrMnO_3$ and (111) NiO planes, while the boundary b - c corresponds to stacking of (110) $LnCrMnO_3$ and (002) NiO planes with the angle of distortion equal to 5.38°. A perovskite-like phase is also present as rather disordered regions situated between the NiO particles (Fig. 5).

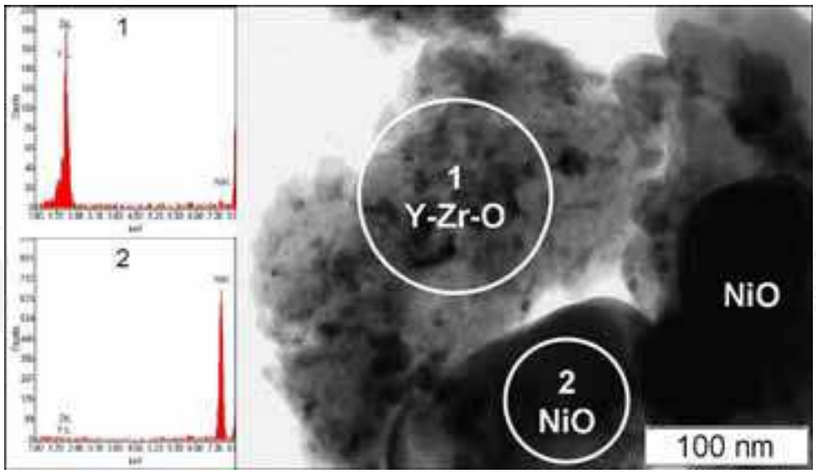

Fig. 1. Typical image of NiO/8YSZ composite I particles with EDX data

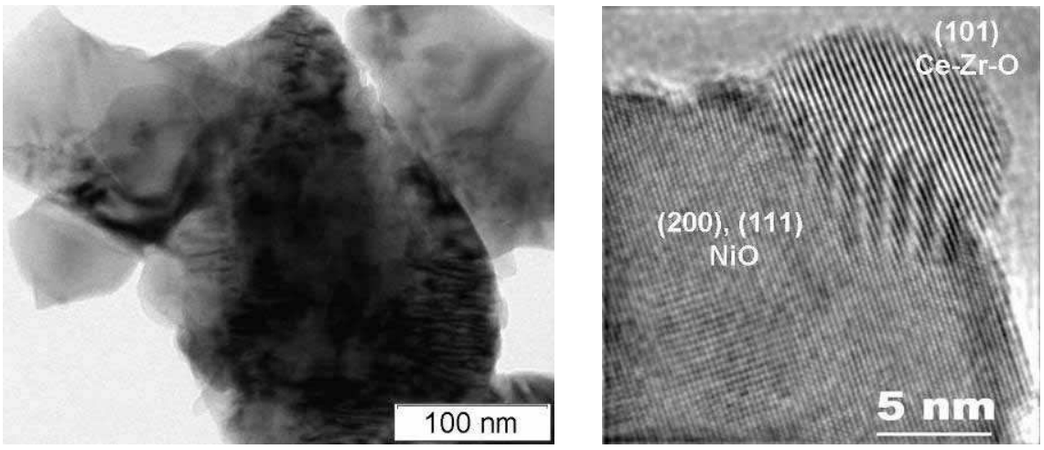

Fig. 2. Typical moire patterns due to perovskite (left) of fluorite (right) layers on NiO particles in composite I.

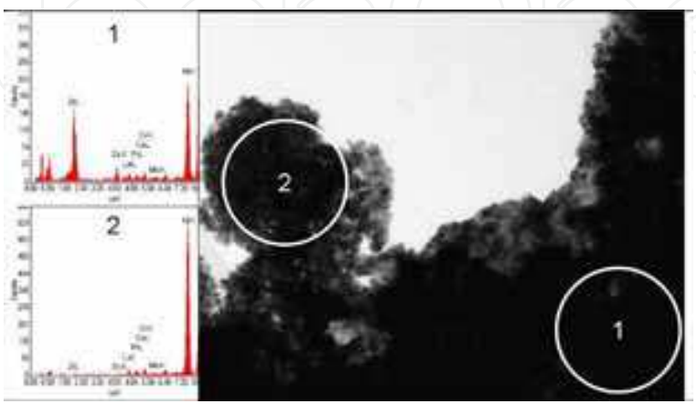

Fig. 3. Typical TEM image of composite III aggregates with EDX data for regions 1 and 2.

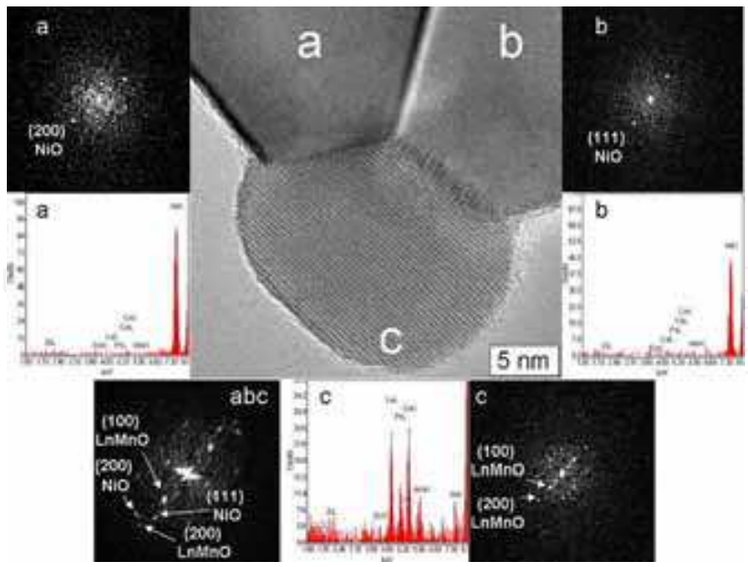

Fig. 4. High resolution image of stacked NiO and perovskite particles in composite III with EDX data for respective regions and DDP from the stacking range. In EDX spectra, CeL subscription refers to the overlapping lines of Ce and Pr.

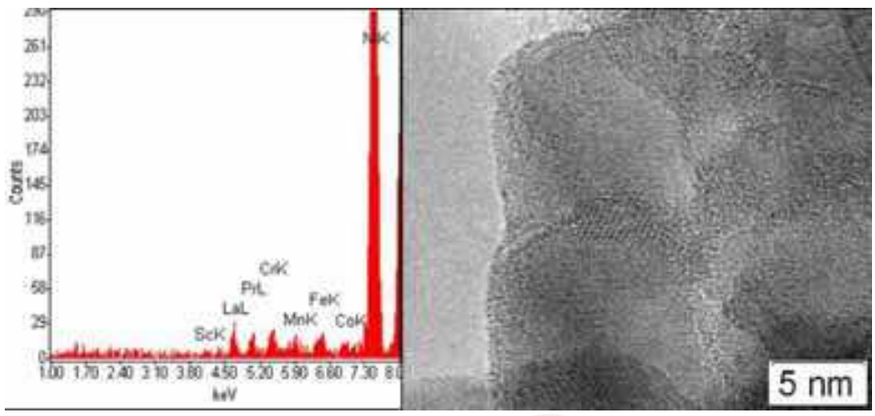

Fig. 5. TEM image of NiO particles with perovskite inclusions between them (right) and respective EDX spectrum from boundary region (left).

Composite III is comprised of big (~1 mkm) porous aggregates formed by stacking of particles with typical sizes in the range of 10–100 nm (Fig. 6a). YSZ particles are comprised of well-crystallized coherently stacked domains with distances 3.02A˚ corresponding to the (111) planes of cubic zirconia [JCPDS 70-4431] separated by nanopores with walls oriented along the lattice planes (Fig. 6b). In other regions (Fig. 6c) juxtaposed NiO and fluorite-like oxide particles containing elements corresponding to cations of doped ceria–zirconia oxide are revealed. A high-resolution image of some regions (Fig. 6d) shows nearly coherently intergrown particles of YSZ and NiO. EDX analysis revealed considerable incorporation of components corresponding to doped ceria–zirconia phase into YSZ, which is also reflected in the increase of (111) spacing to 3.08A˚. Simultaneously, presence of some Ni in EDX spectrum suggests its presence in the surface layer of YSZ, perhaps, as perovskite-like clusters, though its incorporation into the lattice or nanopores of YSZ is possible as well. Traces of Zr and Y were also revealed in the regions of NiO particles.

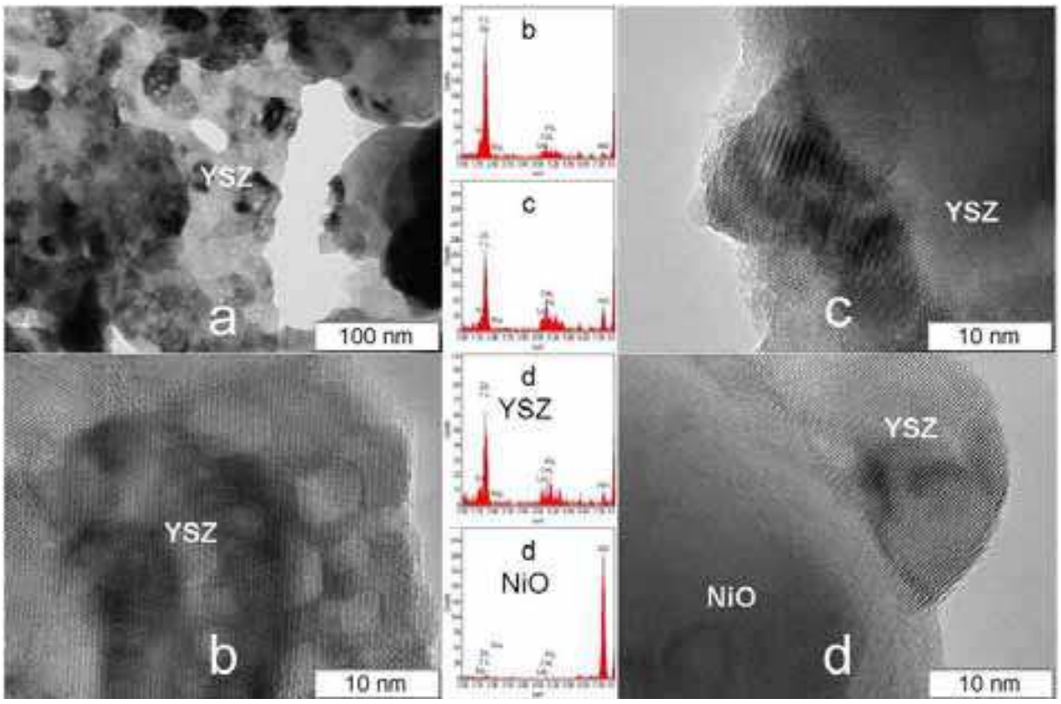

Fig. 6. Typical morphology, microstructure and local composition of composite III promoted by Pr-La-Ce-Zr-O and Ru. (a) macro/mesoporous aggregates of particles; (b) disordered nanodomain ZrO2 particle and respective EDX spectrum; (c) disordered nanodomain particles of fluorite-like oxide promoter on the surface of NiO particle and respective EDX spectrum; (d) contact area between NiO and YSZ particle modified by the elements of complex oxide promoter.

2.1.2 Microstructure of composites with a low content of NiO and YSZ

For these composites prepared via Pechini route, big NiO particles are usually not observed (Fig. 7). Hence, in this case Ni cations appear to be mainly incorporated into the surface layer of the main phase –doped ceria-zirconia or mixed chromate-manganite. There is some non-uniformity in phases/elements distribution in nanocomposites as revealed by EDX. Broad variation of (111) spacing in fluorite-like oxide –from 3.08 to 3.13 Å is apparently caused by variation of the chemical composition of neighboring domains.

For composites with a high specific surface area supported precious metals were usually not observed by TEM as separate particles due to their high dispersion and strong interaction with complex oxides.

Hence, TEM and EDX studies revealed pronounced interaction between phases present in composites reflected in redistribution of elements between constituting phases including surface decoration and incorporation into the surface layers and in the bulk of particles. After testing in the reaction of CH_4 steam reforming in stoichiometric steam/methane feeds, NiO particles are transformed into Ni^o. However, majority of particles remain in a close contact with the particles of complex oxide promoters. In this case their surface remains to be free of carbon. Graphite –like deposits were observed only on the surface of Ni particles not covered by complex oxide promoters (Sadykov et al., 2008b).

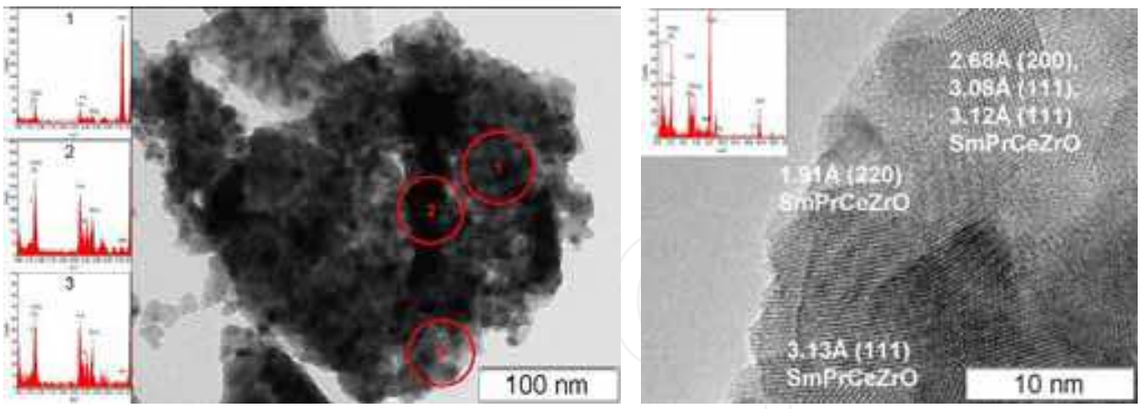

Fig. 7. TEM images and EDX spectra for nanocomposite 1.2%Pt/80%SmPrCeZr+20Ni/YSZ

2.2 X-ray diffraction data

For composites **I** and **II** with a high content of NiO and doped zirconia, strong reflections of these phases and weak broad reflections corresponding to dispersed complex oxide promoters were observed (Sadykov et al., 2008b, 2009b). After testing in the reaction of CH_4 steam reforming in stoichiometric feeds, NiO is completely reduced to metallic Ni. For composite II without supported Pt group metals, a weak broad reflection at $2\theta \sim 27^o$ corresponding to graphitized carbon was observed agreeing with TEM data (Sadykov et al., 2008b, 2009b).

More subtle details were revealed in diffraction patterns of composite **III** and composites with a low content of NiO and YSZ. Thus, for composite **III** both before and after supporting doped ceria–zirconia oxide, along with reflections corresponding to cubic/tetragonal YSZ phase [JCPDS 70-4431] (highly dispersed c- or t-ZrO_2 phases are not discerned easily by routine XRD analysis (Sadykov et al., 2009b), reflections corresponding to monoclinic zirconia phase [JCPDS 78-1807] were observed as well (Fig. 8). As judged by the ratio of reflections intensity, promotion of NiO + YSZ composite by Pr-La-doped ceria–zirconia oxide increases further the content of monoclinic zirconia. This implies that preparation procedure of composite **III,** namely, successive impregnation of YSZ powder with the excess of acidic nitrate solutions followed by evaporation to dryness and calcination (Sadykov et al., 2009b) favors leaching of Y from doped zirconia. This results in destabilization and disordering of the cubic zirconia structure, while at least the surface layers of perovskite-like yttrium nickelates can be formed. Such variation of the structural features of doped zirconia was not observed for NiO + YSZ (ScCeSZ) composites promoted by complex oxides via impregnation with solutions of polymeric polyester precursor (Pechini route) even for samples with a low content of highly dispersed YSZ (Fig. 9). Hence, acidity of impregnation solutions and the time of their contact with YSZ during evaporation appear to play the main role in leaching of Y from YSZ.

Within all uncertainty of estimation of position for rather broad reflections of dispersed doped ceria-zirconia oxide, it remained more or less the same in nanocomposites as in pure oxides (Fig. 9), so redistribution of elements between YSZ and doped ceria-zirconia particles (if any) can be limited to the interfaces. The broadening of doped ceria-zirconia diffraction peaks in nanocomposite and the intensity decline suggest though some disordering of this phase due to the effect of new incoherent interfaces with NiO and YSZ. Note that reflections of NiO phase are very narrow despite its relatively low amount. Hence, at least for NiO particles observed by XRD, their size distribution is to be rather narrow as well.

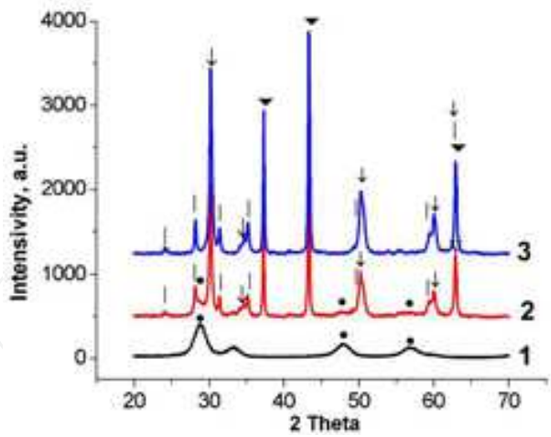

Fig. 8. XRD patterns of $Pr_{0.15}La_{0.15}Ce_{0.35}Zr_{0.35}O_2$ (1), 10% $Pr_{0.15}La_{0.15}Ce_{0.35}Zr_{0.35}O_2$ / NiO + YSZ (2) and NiO + YSZ (3). ●- $Ce_{0.35}Zr_{0.35}La_{0.15}Pr_{0.15}O_2$, | -$Zr(Y)O_2$ monoclinic, ↓-$Zr(Y)O_2$ cubic, ▼- NiO.

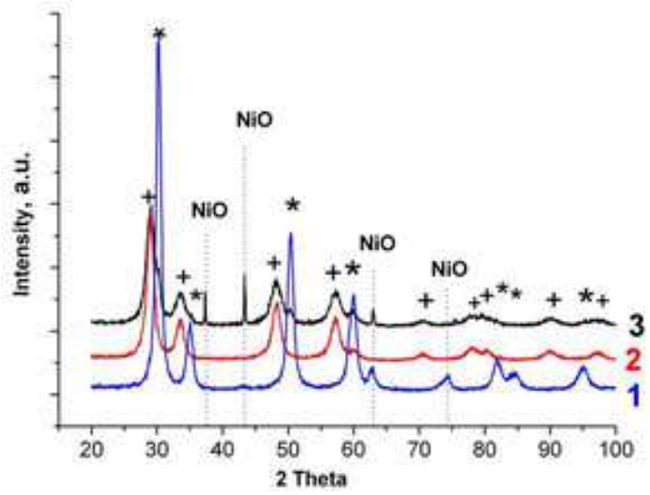

Fig. 9. XRD patterns of $Zr_{0.92}Y_{0.08}O_2$ calcined at 500 °C (1), $Sm_{0.15}Pr_{0.15}Ce_{0.35}Zr_{0.35}O_2$ complex oxide (2) and composite 80% $Sm_{0.15}Pr_{0.15}Ce_{0.35}Zr_{0.35}O_2$/10%NiO/10% $Zr_{0.92}Y_{0.08}O_2$ (3). *-$Zr_{0.92}Y_{0.08}O_2$, +-$Sm_{0.15}Pr_{0.15}Ce_{0.35}Zr_{0.35}O_2$.

For Pt-promoted composites with a low content of NiO, rather narrow reflections corresponding to Pt particles were detected (Fig. 10). As was earlier shown for Pt-supported doped ceria-zirconia nanocrystalline oxides (Sadykov et al., 2007e), only a small part of supported Pt is present as metal particles detected by XRD, while oxidic forms (clusters, Pt^{2+} cations) stabilized due to strong interaction with support dominate. Note that supported Ru is not detected by XRD (Fig. 10) due to a higher stability of its oxidic forms.

Hence, structural studies of nanocomposites comprised of NiO, YSZ, complex oxide promoters and supported Pt group metals revealed pronounced interaction between constituting phases. Decreasing the sizes of constituting phases and modification of preparation procedure favor this interaction manifested as heteroepitaxy, decoration and redistribution of elements between neighboring domains. One-pot Pechini procedure provides the smallest sizes of constituting phases particles, while impregnation with acidic nitrate solutions favor redistribution of elements between phases due to leaching.

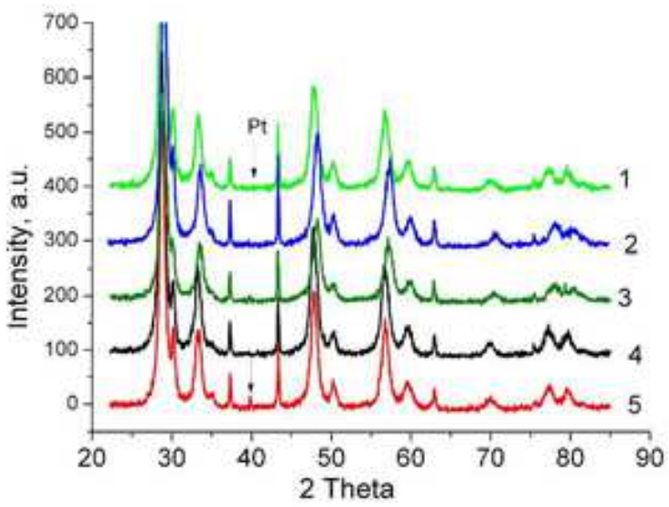

Fig. 10. XRD patterns for some composites containing 10%NiO, 10%YSZ and 80% Sm(Pr)CeZrO promoted by 1wt.% Ru (1,2,4), 0.5wt.% Pt + 0.5wt.% Ru (3) or 1wt.% Pt (5).

3. Reactivity of (nano)composites

3.1 H_2 TPR

Reduction of NiO in composites by H_2 proceeds via the topochemical mechanism, which includes generation of Ni^o nuclei at some specific surface sites (outlets of dislocations etc) with their subsequent growth accompanied by the expansion of reaction area at the NiO/Ni^0 interface (and, respectively, reaction rate increase) until nuclei overlap forming a dense layer of Ni^o product followed then by the reaction rate decline described by a contracting sphere model (Boldyrev et al., 1979). Hence, this reaction is sensitive to the real/defect structure, dispersion and surface composition of NiO particles in green composites, which are of a great importance for understanding the catalytic properties of these systems in steam reforming of fuels. Oxide additives should not cover all the surface of NiO particles by a dense layer to cause noticeable effect on their reduction characteristics. It is sufficient to decorate a small number of surface defect sites in vicinity of the dislocation outlet or domain/grain boundaries to hamper or accelerate removal of oxygen from these sites, and, hence, dynamics of Ni^o nucleation, thus shifting TPR peak position.

Typical H_2 TPR spectra for NiO-doped zirconia nanocomposites, both initial and with supported complex oxides, are shown in Figs. 11, 12. For all samples, NiO reduction was completed up to 600–700 ^oC. For composite I, reduction starts at ~280 ^oC with T_{max} ~ 350 ^oC, which is rather close to typical characteristics for samples of pure NiO or its mechanical mixture with YSZ (Montoya et al., 2000; Sanchez-Sanchez et al., 2007) and agrees with the microstructural data revealing little if any interaction between NiO and YSZ in this case. Supporting Ce–Zr–O oxide on this composite shifts T_{max} to ~400 ^oC, apparently due to a partial blocking of NiO surface (especially surface defects at which nucleation of Ni^o occurs) and/or stabilizing Ni^{2+} cations thus hampering reduction. Indeed, similar position of reduction peak was earlier observed for NiO supported on Ce-Zr-O_2 (Romero-Sarria et al, 2008).

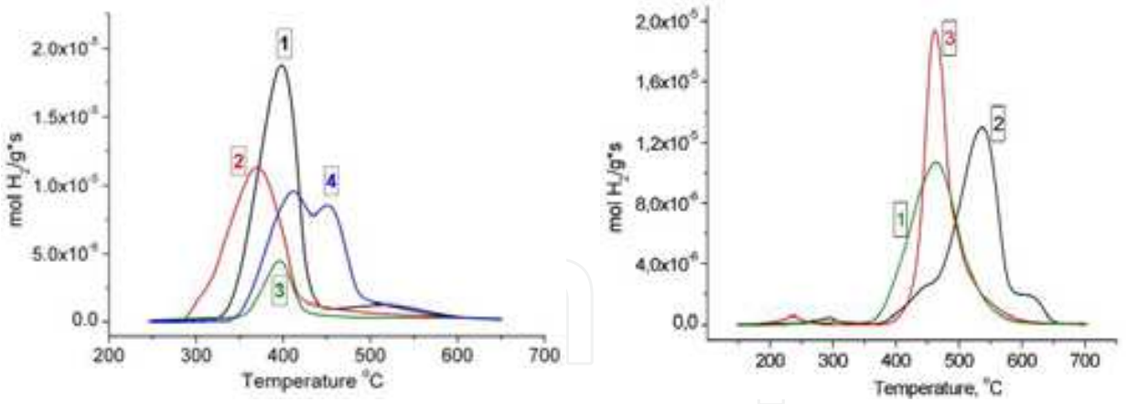

Fig. 11. Typical H_2 TPR spectra for different NiO/YSZ composites promoted by fluorite-like oxides (left) or perovskite-like oxides (right). 5 % H_2 in Ar, 5 l/h, temperature ramp 5°/min. Left: 10% $Ce_{0.5}Zr_{0.5}O_2$/composite I (1), composite **I** (2), composite **VI** (3), 10% SmPrCeZr/composite **III** (4). Right: 0.3% Pd/10% LaPrMnCr/composite **I** (1), composite **II** (2), 0.3% Pd/composite II (3).

For unpromoted NiO + YSZ composite III, reduction starts at ~330 °C and is characterized by three overlapping peaks with T_{max} situated at ~ 350, 400 and 450 °C (Sadykov et al., 2009b). In addition, the high-temperature (up to 700°C) tail of hydrogen consumption was observed for both undoped and doped samples of composite III. The first peak can be assigned to reduction of NiO particles not modified by interaction with YSZ. The second peak is close by position to that in composite I promoted by $Ce_{0.5}Zr_{0.5}O_2$ oxide (Fig. 11), so it can be similarly explained by decoration of the surface of NiO particles with irreducible $Y(Zr)O_x$ oxidic species. Indeed, TPR peaks with T_{max} situated even at higher (450–600°C) temperatures were observed in the case of NiO supported on zirconia, ceria–zirconia or alumina (Montoya et al., 2000; Srinivas et al., 2003; Matsumura & Nakamori, 2004). By analogy with these data, the high-temperature tail of hydrogen consumption can be assigned to reduction of Ni cations incorporated into the bulk of doped zirconia particles (vide supra). Hence, TPR data revealed pronounced variation of the reactivity of NiO particles/species even in unpromoted NiO + YSZ composites, which could reflect different degree of chemical interaction between components.

Supporting doped ceria-zirconia complex oxides on composite III practically eliminates the first TPR peak situated at ~350°C (Fig. 11), slightly shifts the second peak to higher temperatures and increases the relative share of the high -temperature peak at ~470°C. A high-temperature reduction tail remains to be observed for all samples. This implies that the second impregnation provides modification of the surface of all NiO particles present in composite by Zr and rare-earth cations.

For composite VI prepared via Pechini route with the same type of PrSmCeZrO complex oxide additive and having much smaller content of NiO and YSZ only one H_2 TPR peak (Fig. 11, curve 3) was observed. A lower intensity of this peak as compared with that for other samples (curves 1 and 4, Fig. 11) correlates with a smaller NiO content, while its position is rather close to that for other peaks assigned to reduction of NiO particles decorated by fluorite-like oxides . This suggests that reactivity and lattice oxygen mobility of small NiO particles strongly interacting with complex fluorite-like is rather close to that of bulky particles decorated with fragments of fluorite-like oxides.

Complex perovskite oxide strongly hampers NiO reduction in the composite I (Fig. 11, curve 1): reduction peak shifts to ~460ºC even despite co-promotion with Pd. This is explained by the relatively low reducibility/lattice oxygen mobility of complex manganochromite (Peña-Martínez et al., 2006; Sfeir et al., 2001; Sauvet & Irvine, 2004) rather uniformly covering the surface of NiO particles in this composite thus hampering reduction. For composite II also containing complex perovskite phase as an additive and prepared via one-pot Pechini route, the reduction peak is shifted to even higher (~530ºC) temperatures (Fig. 11, curve 2). In agreement with TEM data (vide supra) this suggests even stronger interaction between the perovskite and NiO particles in this sample. Appearance of the high-temperature shoulder at ~600ºC implies that some Ni cations could be even incorporated into the bulk of perovskite particles/domains thus forming Ni-substituted oxide (Sauvet & Irvine, 2004; Sfeir et al., 2001). Promotion of this composite with a small amount of Pd shifts reduction peak to lower temperatures and removes high-temperature shoulder (Fig. 11, curve 3).

In general, promoting effect of supported Pt group metals on the oxides reduction by hydrogen is a well-documented phenomenon explained by the efficient activation of H_2 molecules on the metal particles and spill-over of atomic hydrogen onto the oxide surface, thus easily removing reactive oxygen forms (Bernal et al., 2002). Downward shift of H_2 TPR peak is observed for any mechanism of the solid oxide reduction, either topochemical (such as NiO reduction) or diffusion-controlled (reduction of ceria–zirconia solid oxide solution). Facilitation of the lattice oxygen mobility due to incorporation of precious metals into domain boundaries and subsurface layers is demonstrated as well (Sadovskaya et al., 2007).

Promotion of composites by Ru or Pt clearly accelerates their bulk reduction by hydrogen (Figs. 12) characterized by the main peak situated at 370–400ºC. In addition, in the low-temperature (100–300ºC) range, new peaks appear apparently corresponding to reduction of different Ru and/or Pt oxidic species accompanied by reduction of complex fluorite-like oxides. For Ru supported on ceria or zirconia, peaks assigned to reduction of RuO_2 species with different dispersion are situated at 80–100ºC [Hosokawa et al., 2003; Yan et al., 2007). For Pt-supported Pr-Ce-Zr-O samples, reduction starts at ~ 150ºC with the main maximum situated at ~ 280ºC and a shoulder at ~ 200ºC (Sadykov et al., 2007e). Hence, TPR peaks at 115–150ºC observed for Ru-promoted samples of composites with a high NiO/YSZ content (Sadykov et al., 2009b) suggest rather weak interaction of RuOx species with other phases present in composites. When Ru cations are incorporated into the surface vacancies of La–Sr–chromate with the perovskite structure, these peaks are shifted to higher (180–200ºC) temperatures (Yan et al., 2007). Hence, peak observed at ~200ºC for nanocomposite with a high (80%) content of Pr-Ce-Zr-O fluorite can be assigned to reduction of RuO_x species strongly interacting with this oxide, perhaps, modified also by dissolved Ni cations (Fig. 12).

This interaction apparently facilitates reduction of NiO present in promoted composites, since T_{max} of the main reduction peak is shifted downward. For Pt-supported nanocomposite (Fig. 12), position and shape of the low-temperature peak is practically the same as that observed for Pt/Pr-Ce-Zr-O samples (Sadykov et al., 2007e). Intermediate position is observed for Pt+Ru-promoted samples (Fig. 12) suggesting formation of mixed PtRuOx oxidic species.

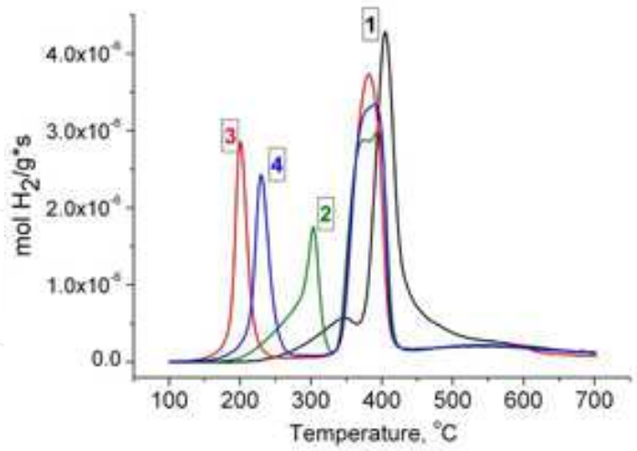

Fig. 12. H_2 TPR spectra of 80%$Pr_{0.3}Ce_{0.35}Zr_{0.35}$ +10NiO+10YSZ composite (1) promoted with 1wt.%Pt (2), 1wt.% Ru (3) or 0.5wt.% Pt + 0.5wt.% Ru (4)

3.1 TPR by fuel molecules (CH_4, C_2H_5OH) and reoxidation by H_2O

Temperature-programmed reduction of composites by fuels (methane, ethanol) followed by reoxidation with H_2O characterizes mobility and reactivity of oxygen species and provides also an additional information on ability of surface sites to activate reagents.

3.1.1 CH_4 TPR

Reduction of bulk NiO sample (a starting compound for preparation of composite I) starts at ~400°C and occurs in a narrow (~100°C) temperature range with practically simultaneous appearance of deep (CO_2, H_2O) and partial (CO, H_2) oxidation products (Fig. 13). While CO_2 evolution rapidly falls to zero, other products are observed up to 800°C. H_2 evolution declines to zero when sample is completely reduced. This means that bulk Ni^0 particles are not able to continuously dissociate CH_4, aparently due to a rapid surface blocking by the graphitic carbon.

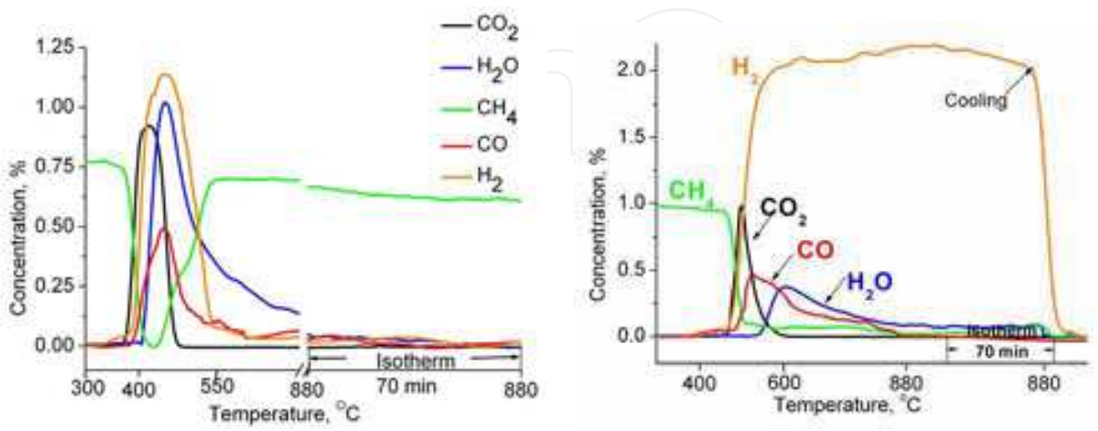

Fig. 13. Typical CH_4 TPR data for NiO (left) and nanocomposite **III** (right). Experimental parameters for Figs. 13-14: contact time 0.1 s, 1% CH_4 in He, temperature ramp 5°/min.

For undoped composites, reduction by CH_4 starts at higher than for pure NiO temperatures (Fig. 13), which agrees with H_2 TPR data (vide supra) and is explained by migration of irreducible cations from YSZ onto the surface of NiO. Some H_2 evolution continues even after complete reduction of composites due to CH_4 decomposition. This suggests that interaction between components even in undoped composites prevents formation of a dense layer of graphitic carbon.

Doping by complex oxides and Pt group metals facilitates the reduction shifting TPR peaks to lower temperatures (Fig. 14). This is explained by a higher efficiency of Pt group metals in C-H bond dissociation as compared with the centers of NiO or fluorite-like/perovskite-like oxides. Indeed, reduction of doped ceria or ceria–zirconia oxides by methane starts from ~400ºC with evolution of deep oxidation products followed by syngas generation at higher (>700ºC) temperatures (Sadykov et al., 2007a). As far as CH_4 pyrolysis is concerned, there appears to be some synergy between the action of Pt group metal, complex oxide additive and Ni. Hence, interaction between components in nanocomposite apparently helps to prevent formation of dense graphitic layers in the course of CH_4 pyrolysis. Polymerized $C_xH_yO_z$ species inevitably formed on the surface of nanocomposites due to this pyrolysis appear to possess more loose structure due to incorporation of oxygen atoms. Reoxidation of deposited coke by H_2O revealed that for Pt-supported doped ceria–zirconia sample CO_2 evolution in the course of H_2O oxidation starts at temperatures below 400ºC without any evolution of H_2 up to ~ 550ºC (Fig. 15). It clearly can be explained only by decomposition of some surface carbonate complexes –either organic ones within coke precursors or inorganic ones. The maximum of CO, CO_2 and H_2 evolution due to oxidation of coke by water accompanied by simultaneous reoxidation of doped ceria--zirconia is situated at ~ 880ºC (Fig. 15). For Ni/YSZ composites, both promoted or not, oxidation of deposited during CH_4 TPR runs carbonaceous species accompanied by simultaneous CO_2, CO and H_2 evolution starts earlier and proceeds faster than for Pt-supported fluorite-like oxides (Fig. 15). This suggests involvement of Ni surface atoms together with Pt in gasification of the surface coke. Indeed, while Ni atoms can be oxidized by H_2O producing hydrogen and oxygen atoms, it is impossible for Pt atoms. So, the function of Ni in this case is to provide efficient activation of mild oxidant- water at temperatures lower than those typical for reduced doped ceria-zirconia oxide. On the other hand, Pt atoms could use these oxygen atoms supplied to them via spillover for the efficient oxidation of coke precursors.

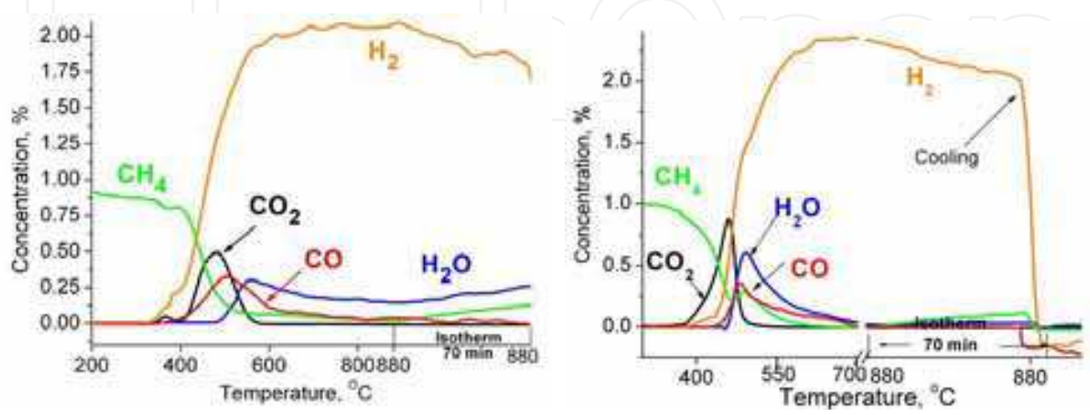

Fig. 14. Typical CH_4 TPR data for samples of 1.4Pt/10$Pr_{0.15}Sm_{0.15}Ce_{0.5}Zr_{0.2}O_2$/composite III (left) and 1Ru/10LaMnCrPr/compositeV.

Another new feature revealed in these experiments is evolution of CH_x (or, in general, hydrocarbons) in the process of H_2O TPO of reduced and coked promoted composite (Fig. 15). This supports hypothesis that complex oxide promoters make deposited coke species less dense and, perhaps, containing a bigger fraction of hydrogen atoms (Sadykov et al., 2008b), so they are more easily cracked by interaction with the surface hydroxyls.
In H_2O TPO spectra of both promoted and unpromoted composites (Fig. 15) peaks of CO_2 evolution in the isothermal mode at 880°C are present. A similar by position peak is present in the H_2O TPO spectrum of Pt-supported coked doped ceria-zirconia oxides (Fig. 15, left). Hence, its appearance in the case of nanocomposites TPO spectra can be explained by oxidation of a part of carbonaceous species located on the surface of YSZ or doped ceria-zirconia particles remote from the interface with Ni particles.

3.1.2 C_2H_5OH TPR

In these experiments, to prevent condensation of unreacted ethanol and its partial oxidation products in the gas analyzer, a cooled to -40°C trap was situated at the reactor exit. This precludes estimation of carbon balance and degree of ethanol conversion. However, analysis of dynamics of products evolution allows to make useful conclusions about reactivity and route of transformation of ethanol for different types of composites.
Figs. 15, 16 show typical results of ethanol TPR experiments for composites with broadly varying compositions. In general, their reactivity with respect to ethanol is comparable: at ~ 300°C H_2 appears followed by other products including H_2O, CO_2, CO and CH_x. While CO_2 and H_2O are products of ethanol oxidation by the lattice oxygen of composites, CH_x is comprised of non-condensed products passed through the trap such as CH_4 and C_2H_4 formed due to cracking and dehydration of ethanol (de Lima et al., 2008). After complete reduction of catalysts, evolution of H_2 and CO continues due to decomposition of ethanol (Domine et al., 2008). Though it is inevitably accompanied by accumulation of surface carbonaceous species, however, within the time scale of experiments, performance is stable which suggests deposition of loose coke species. Since in all cases at the steady state the H_2/CO ratio in the products is close to 2.5, by stoichiometry of ethanol decomposition this coke should retain a lot of hydrogen atoms. CH_x formation due to ethanol cracking continues only in the case of composites containing doped ceria-zirconia oxides (Fig. 15, left). In studied conditions concentrations of CO (~0.5-0.75%) and H_2 (~ 1.25-1.75%) were rather close for studied composites.
Temperature-programmed reoxidation by H_2O of deposited carbonaceous species starts at rather low (~ 400°C) temperatures and proceeds fast (Fig. 16). Hence, for nanocomposites containing even relatively low content of complex oxide promoters carbonaceous deposits derived from ethanol are highly reactive, which is one of the criteria of stability of these composites performance in steam reforming of ethanol (de Lima et al., 2008).

4. Catalytic activity in SR of CH_4 and biofuels

4.1 Catalytic properties of dispersed nanocomposites in methane steam reforming

4.1.1 Composites with fluorite-like oxide additives.

Typical values of CH_4 conversions for different nanocomposites and estimated from these values effective first-order rate constants are given in Figs. 17, 18 and Table 1.

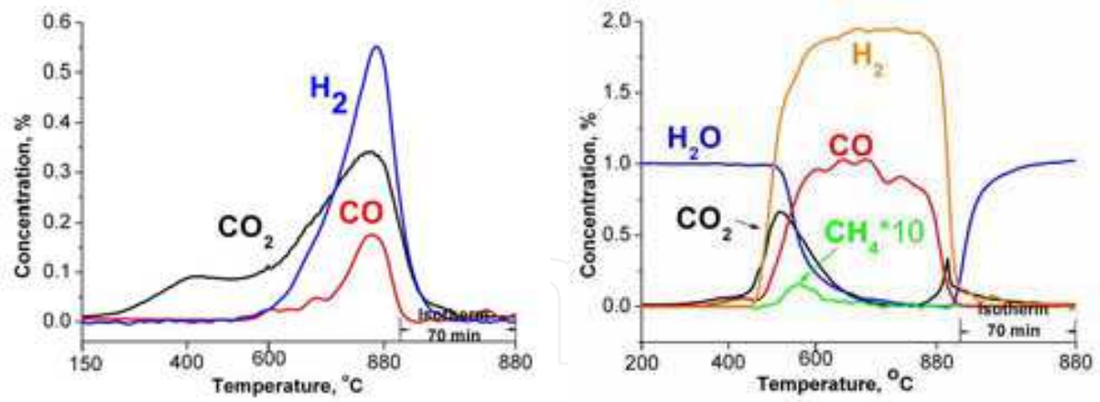

Fig. 15a. Temperature-programmed oxidation by H_2O of reduced and coked in CH_4 TPR runs samples of 1.4 wt.% $Pt/Pr_{0.15}Sm_{0.15}Ce_{0.5}Zr_{0.2}O_2$ (left) and 1.4 wt.% $Pt/Pr_{0.15}Sm_{0.15}Ce_{0.5}Zr_{0.2}O_2$ /composite III (right) samples. 1% H_2O in He, 5°/min, 0.1 s.

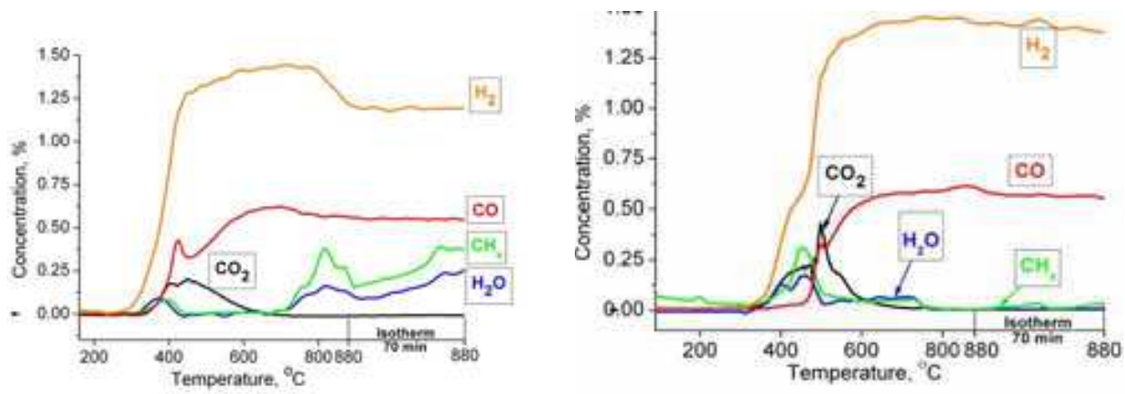

Fig. 15b. Typical EtOH TPR spectrum for sample of nanocomposite series **VI** promoted with 80%SmPrCeZr (left) and nanocomposite series **V** promoted by 80%LaPrMnCr (right). Experimental conditions for Figs. 15-16: 1% EtOH in He, contact time 0.1 s, temperature ramp 5°/min.

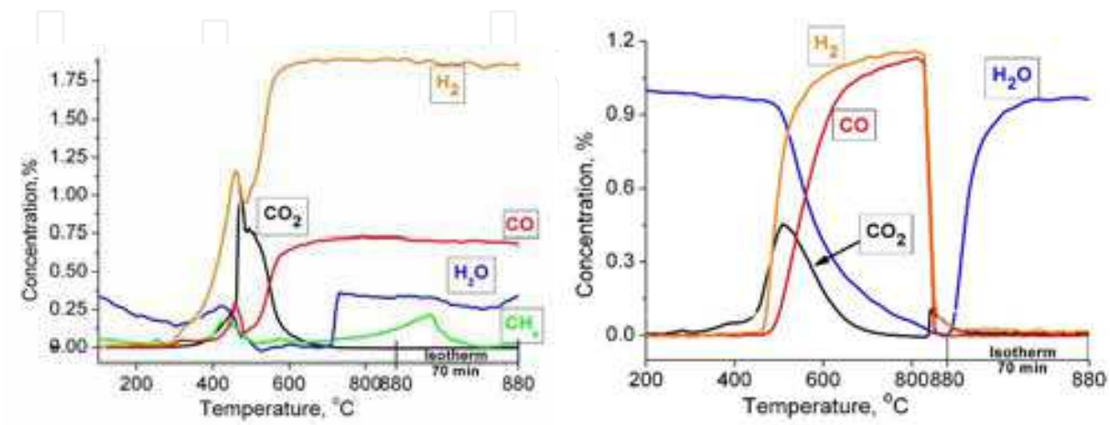

Fig. 16. EtOH TPR (left) followed by H_2O TPO (right) for nanocomposite series **V** promoted by 1%Ru and 10%LaPrMnCr.

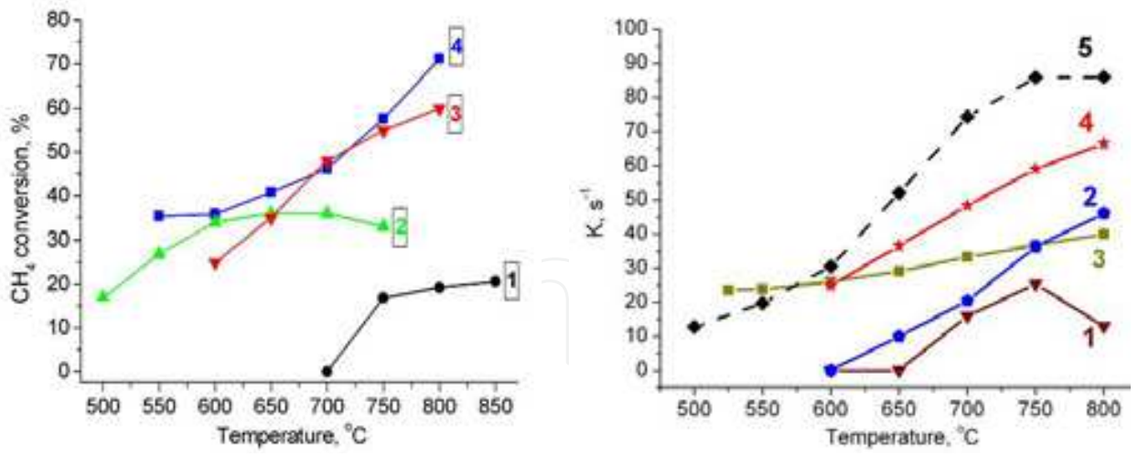

Fig. 17. Temperature dependence of CH_4 conversion (left) and effective first-order rate constants (right) for different composites at 10 ms contact time. Left: 1- 10 wt.% $Pr_{0.3}Ce_{0.35}Zr_{0.35}O_2$/composite **III**, 2-1.3 wt.% Ru/10 wt.% $Pr_{0.15}La_{0.15}Ce_{0.35}Zr_{0.35}O_2$/composite **III**, 3-0.3 wt.% Pt/10 wt.% $Pr_{0.3}Ce_{0.35}Zr_{0.35}O_2$/composite **I**, 4- composite **IV**. Feed 8% CH_4+ 8% H_2O in Ar. Right: 1-composite **I**, 2-$Ce_{0.5}Zr_{0.5}O_2$/composite **I** , 3-0.3%Pd/10%$Ce_{0.5}Zr_{0.5}O_2$/composite **I**, 4,5-0.3%Pt/10% $Pr_{0.3}Ce_{0.35}Zr_{0.35}O_2$ /composite **I**. Feed 8% CH_4+ 8% H_2O (1-4) or 8% CH_4+ 24%H_2O (5).

Supporting complex ceria-zirconia oxides increases catalysts performance at temperatures exceeding 600ºC and stabilizes it at high temperatures (Figs. 17, Table 1) apparently due to hampering of coking. Some samples based upon fluorite oxides promoted composite **III** remain inactive at 650ºC (Table 1), while composite **IV** demonstrates a good performance starting already from 550ºC (Fig. 17). This can be explained both by a higher specific surface area of composite **IV** as well as by a higher degree of interaction between components of this composite provided by one-pot Pechini route of synthesis, and, hence, stabilization of small active Ni clusters on the surface of oxidic components of composite (vide supra).

For the stoichiometric feed, Pd as co-promoter further increases performance of ceria-zirconia promoted composite **I** (Fig. 17, Table 1) making it highly active even at temperatures below 600ºC. Pt as co-promoter also ensures a high activity in the middle-temperature range (Fig. 17, Table 1). Indeed, at 650ºC, effective first –order rate constants estimated for the plug-flow reactor are as high as 30-40 s^{-1} (Fig. 17). Hence, more efficient activation of CH_4 molecules on Pt or Pd clusters demonstrated by CH_4 TPR experiments allows to increase the overall performance of Ni-containing catalysts in the intermediate temperature range, while dispersed fluorite-like oxide promoter along with Ni apparently plays the major role in activation of water molecules and transfer of activated oxygen-containing species (hydroxyls, hydroxocarbonates) to the sites where activated CH_x species are located, thus preventing formation of coke.

The performance of samples co-promoted with Pt and fluorite-like oxides tends to increase in feeds with the excess of steam (Figs. 17, Table 1). This is important from the practical point of view since in real SOFC operation conditions, the oxygen ions transfer through the cell increases the overall content of oxidants within the porous composite anode. The increase of steam content in the feed increases the rate of activated hydrocarbons species transformation into syngas, thus preventing the surface coking and ensuring a high performance of composite co-promoted with Pt and fluorite-like oxide. For Pt as a co-promoter, the effect of the steam excess in feed strongly depends on the exact chemical

Composition	CH_4 conversion, %	
CH_4 : H_2O	1:1	1:3
$Ce_{0.5}Zr_{0.5}O_2$/composite **I**	23	
1.4 wt% Pt/$La_{0.3}Ce_{0.35}Zr_{0.35}O_2$	15	14
0.3 wt.% Pd/$Ce_{0.5}Zr_{0.5}O_2$/composite **I**	43	0
0.3 wt% Pt/$La_{0.3}Ce_{0.35}Zr_{0.35}O_2$ /composite **I**	30	26
0.3 wt.% Pt/$Pr_{0.3}Ce_{0.35}Zr_{0.35}O_2$ /composite **I**	35	50
1.03 wt.% Pt/$Pr_{0.3}Ce_{0.35}Zr_{0.35}O_2$ /composite **I**	0	52
0.5 wt.% Ru/$Pr_{0.3}Ce_{0.35}Zr_{0.35}O_2$ /composite **I**	12	24
0.3 wt.% Pd/LaMnCrPr/composite **I**	26	12
1 wt.% Ru/LaMnCrPr/composite **I**	70	
$Pr_{0.3}Ce_{0.35}Zr_{0.35}O_2$/composite **III**	0	
1 wt.% Ru/$Pr_{0.3}Ce_{0.35}Zr_{0.35}O_2$/composite **III**	32	
1 wt.% Ru/$Pr_{0.15}La_{0.15}Ce_{0.35}Zr_{0.35}O_2$/composite **III**	36	
1 wt.% Ru /$Pr_{0.15}Sm_{0.15}Ce_{0.5}Zr_{0.2}O_2$/composite **III**	19	
Composite **IV** (10$Pr_{0.15}La_{0.15}Ce_{0.35}Zr_{0.35}O_2$ +55NiO +35YSZ)	40	
Composite **V_1** 10LaPrMnCr+90Ni/YSZ (4.1 m^2/g)	21	
Composite **V_2** 50LaPrMnCr+50Ni/YSZ (8.1 m^2/g)	20	
Composite **V_3** 80LaPrMnCr+20Ni/YSZ (12 m^2/g)	22	
1%Ru/composite **V_1** (3 m^2/g)	70	
1%Ru/composite **V_2** (8.9 m^2/g)	45	32
1%Ru/composite **V_3** (6.2 m^2/g)	18	
0.7 % Ru/composite **V_2**		72*

Table 1. Values of CH_4 conversion for CH_4 SR at 650°C on composites promoted with fluorite/perovskite-like oxides and Pt, Pd or Ru. 10 ms contact time,; 1:1 feed (8% CH_4+ 8% H_2O in He), 1:3 feed (8% CH_4+ 24% H_2O in He) and 1:2 feed* (20% CH_4 + 40% H_2O, Ar balance).

composition of the oxide additive. Thus, for sample co-promoted with La-Ce-Zr-O oxide, the effect of the steam excess is small, while for combination of Pt with Pr-Ce-Zr-O oxide additive, this effect is well pronounced (Fig. 17, Table 1).

Note also that for Pt-supported fluorite-like oxides without Ni addition performance is independent upon the water excess (Table 1). A non-additive increase of performance due to supporting Pt along with fluorite-like oxides on Ni-containing composite (a synergetic effect) is thus apparent.

For Pd supported on a composite promoted by ceria-zirconia, the increase of steam content in the feed suppresses the low-temperature performance (Table 1), which could be explained by stabilization of less reactive oxidized Pd species by fluorite-like oxide. Here the main role is played by a higher stability of Pd oxidic forms (perhaps, some surface phases including both Pd and Ce cations) as compared with those of Pt. A lower ability of oxidized Pd species to activate methane is thus responsible for a low activity in feeds with the steam excess.

For Ru as a co-promoter of composite **I** in combination with the fluorite-like oxides, the excess of steam also positively affects the low-temperature performance (Table 1). However, this performance is lower than for Pt-containing samples in all feeds, so Pt is more efficient co-promoter than Ru in combination with complex fluorite-like oxides. This can be explained by a higher efficiency of Pt in activation of methane (Wei & Iglesia, 2004).

For samples promoted by the same amount of Pt, activity is also higher for sample with a higher Ni content despite a lower specific surface area. Hence, the efficiency of the composite in CH_4 SR is defined by the content of components (Ni, Ru, Pt) activating fuel molecules. On the other hand, when Pt or Pd are supported on Ni/YSZ composite without oxide additives, methane conversion is not improved (Sadykov et al, 2006c). This suggests that namely combination of precious metals with oxide promoters helps to provide enhanced activity of composites in the intermediate temperature range. Due to a low content of supported precious metals, their effect can be assigned to modification of some specific defect centers of Ni particles. This suggestion agrees with a high performance of composite **IY** prepared via one-pot Pechini synthesis procedure (Fig. 17) even without promotion by precious metals.

The synergy of the catalytic action of components in nanocomposites is retained for feeds with the excess of steam. Thus, for nanocomposites containing Pt and SmPrCeZr as co-promoters, sample with a higher Ni content provides significantly higher CH_4 conversion in the whole temperature range in both stoichiometric (1:1) and more oxidizing (1:3) feeds (Fig. 18). At a low Ni content, the excess of steam provides a higher CH_4 conversion in the whole temperature range due to efficient activation of CH_4 on Pt sites remaining in the metallic state even in the oxidizing conditions. At a high Ni content, a complex temperature – dependent effect of the steam excess on activity suggests interplay of several factors determined by interaction between Pt, Ni and fluorite-like oxide and affecting efficiency of CH4 and H_2O activation and, hence, steady-state oxidation degree of Ni surface and its coverage by coke.

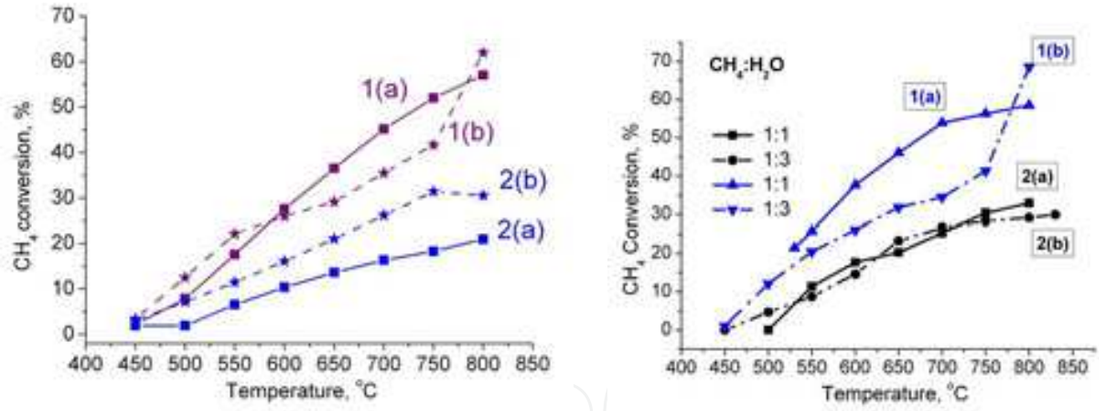

Fig. 18. Effect of water excess in the feed on performance of nanocomposites promoted by Pt and SmPrCeZr (left) or Ru and LaPrMnCr (right) in)) in CH_4 SR an H_2O/CH_4 =1 (a) or 3(b). Contact time 10 ms, CH_4 concentration 8%. Left: 1-Pt/10SmPrCeZr/Ni/YSZ, 2-Pt/80SmPrCeZr/Ni/YSZ. Right: 1- Ru/50LaPrMnCr/Ni/YSZ, 2- 50LaPrMnCr/Ni/YSZ.

4.1.2 Composites with perovskite-like oxide additives

Ni/ScCeSZ cermet without oxide promoters was not able to provide a steady-state performance in the methane SR in stoichiometric feeds due to very fast coking leading finally to the reactor plugging (Sadykov et al., 2006c, 2008b). After reduction by H_2, composite **II** comprised of Ni/ScCeSZ cermet promoted by perovskite-like oxide demonstrates a reasonably high and stable activity at temperatures exceeding 650ºC (Sadykov et al., 2008b). Similarly, promotion of composite **I** by perovskite oxide allows to obtain a reasonable

performance in methane steam reforming even at 650 ^{o}C (Table 1). By itself, La-Pr-Mn-Cr-O perovskite is inactive in SR of methane. However, incorporation of Ni cations into the lattice of such irreducible perovskites provides a reasonable level of activity in methane steam reforming (Sauvet & Irvine, 2004). Hence, observed high and stable activity of perovskite-promoted composites in CH_4 SR in stoichiometric feed can be explained by a partial dissolution of NiO in the acidic polyester solution at the preparation stage. At subsequent calcination, Ni-containing perovskite is formed (vide supra EDX data). Under contact with reducing reaction media, small highly reactive Ni clusters are segregated on the surface of perovskite oxide being stabilized by interaction with this matrix stable in reducing conditions. In addition, the surface of big NiO particles in non-reduced composite is covered by the perovskite layers (vide supra). Hence, big Ni^0 particles generated due to NiO reduction in the reaction media are decorated by perovskite-like oxidic species. A high efficiency of these species and/or separate perovskite particles in activation of steam and carbon dioxide facilitates gasification of CH_x species produced by methane activation on Ni, thus preventing coking. This level of high-temperature activity for perovskite-promoted composite **I** (Table 1) is close to that provided by ceria-zirconia oxide promoter. Hence, similar factors affecting surface properties of Ni particles in promoted composites as well as enhanced activation of water and/or CO_2 molecules on the surface sites of oxide additives could operate in the case of both types of oxide promoters ensuring high and stable performance of composites in methane SR in stoichiometric feeds, especially at rather high (>700^{o}C) temperatures.

The increase of steam/methane ratio from 1 to 3 was found to decrease the high –temperature performance of perovskite-promoted composite **I** (Sadykov et al., 2006c, 2008b). This can be assigned to partial oxidation of Ni surface atoms contacting with perovskite species/particles and their stabilization as less active perovskite–like fragments.

Co-promotion of composites with perovskite-like oxide and Ru allowed to achieve a high level of middle-temperature activity in feeds with different steam/methane ratios (Table 1, Fig. 18). For composite **II**, the increase of Ru content from 0.3 to 1 wt.% decreases activity in the stoichiometric feed and increases it in the feed with the excess of steam (Sadykov et al., 2010b). This behavior can be explained by a higher rate of CH_4 activation on the surface of sample with a higher Ru content, thus leading to deactivation due to coking in stoichiometric feed. In a feed with the excess of steam, enhanced rate of activated CH_x species gasification prevents coking and provides a higher performance of sample with a higher Ru content due to a higher rate of CH_4 activation. Similar features observed for composite **I** co-promoted with fluorite-like oxide and Pt (Table 1) agree with this explanations of the precious metal content and feed composition effects.

For composites series **V** containing LaPrMnCr and promoted by 1%Ru (Table 1), activity increases with Ni content, thus clearly demonstrating synergy of Ni+ Ru action due to suppression of coking ability of Ni sites explained by the surface alloys formation. Activation of H_2O molecules on Ni atoms can be important as well.

As follows from Fig. 18, Ni/YSZ cermet promoted only by perovskite –like complex oxide provides the same CH_4 conversion in both types of feed, while co-promoting effect of Ru is much stronger in the stoichiometric feed. This suggests that in feed with the steam excess Ru is in part transformed into less active oxidic forms stabilized by perovskite-like complex oxide.

When comparing two series of samples co-promoted with precious metals and either fluorite-like or perovskite-like oxides (Table 1), the middle-temperature performance of the best samples of both series is comparable. For samples promoted with perovskite-like oxide,

the highest activity is provided by supporting Ru, while for samples with fluorite-like oxide additives, the highest performance is observed after loading Pt. Hence, these two types of systems can be considered as promising for the practical application. In general, a better performance is provided by YSZ-containing catalysts (Sadykov et al., 2010b). Though more detailed studies are required for elucidating the exact role played by the rare-earth cations in determining catalytic properties of these nanocomposites, it is clear that observed trends are not determined by the oxygen mobility in doped zirconia particles which is higher for ScCeSZ (Smirnova et al., 2007).

Hence, the most efficient promoter for Ni/YSZ –based composite catalyst is Pr(Sm)-doped ceria-zirconia in combination with Pt. Since Pt is more expensive than Ru, the latter was also used as a co-promoter in combination with either perovskite or fluorite oxide when supporting thin layers of NiO+YSZ-based nanocomposites on different substrates (vide infra).

As far as the preparation procedures are concerned, one-pot Pechini route apparently provides the highest activity of promoted composites, at least, for systems with complex fluorite-like oxide additives. Hence, this method was selected as a basic one for preparation of dispersed promoted composites for subsequent supporting on different substrates. As follows from Fig. 19, performance of nanocomposite active components prepared via this route is sufficiently stable in feeds with a small excess of steam.

Temperature-programmed oxidation of nanocomposite samples discharged from reactor after testing in stoichiometric feeds demonstrated that combined action of precious metals and complex oxides decreases the amount of deposited carbon providing thus high and stable performance (Sadykov et al., 2006c, 2008b).

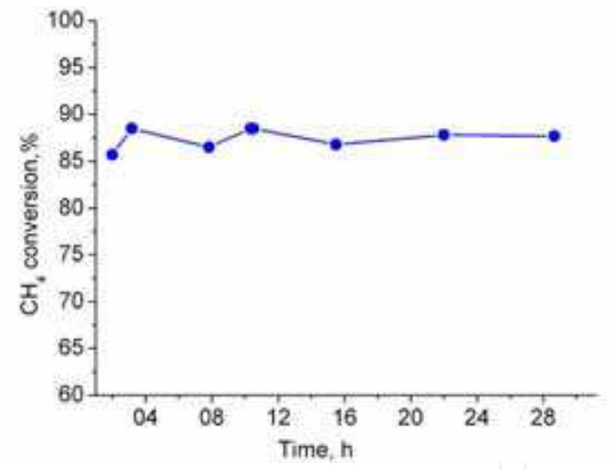

Fig. 19. Stability test for nanocomposite 10%$Sm_{0.15}Pr_{0.15}Ce_{0.35}Zr_{0.35}$+ 55%NiO+35%YSZ +1.4%Pt at 600 °C, feed 20% CH_4 + 40% H_2O, Ar balance, contact time 60 ms.

4.2 Catalytic properties of dispersed nanocomposites in ethanol steam reforming

In this reaction, in general, in the middle-temperature range, activity of all composites, promoted by Ru or not, was rather high (Table 2, Fig. 20). This is explained by a high activity of Ni in this reaction provided coking of its surface is hindered by oxidic promoters. Moreover, specific activity of Ni supported on alumina is reported to be even higher than that of low-loaded Ru (Fatsikostas et al., 2002; Haryanto et al., 2005; Sanchez-Sanchez et al., 2007). This agrees with the results of Srinivas et al. (Srinivas et al., 2003) demonstrating a

high and stable activity in ESR of composites comprised of 40wt. % NiO and 60 wt.% CeO_2 (CeO_2-ZrO_2) prepared via hydrothermal route. Hence, promoted nanocomposites efficient and stable in steam reforming of methane are also quite promising for the steam reforming of ethanol. As can be inferred from the hydrogen content in converted feed, at 700 ^oC, even at short contact time, up to 70% of ethanol is converted along the steam reforming route. C_2H_4 and CH_4 were not revealed in the products, while they were inevitably present for catalysts comprised of precious metals supported on alumina (Erdőhelyi et al., 2006; Romero-Sarria et al., 2008). Hence, for developed composites containing YSZ and complex fluorite-oxide promoters, primary route of ethanol transformation into syngas apparently does not include ethanol dehydration or cracking. This agrees with very high CO_2/CO ratio in products at 700 ^oC in diluted feed clearly not conforming to the equilibrium composition of converted feed (Erdőhelyi et al., 2006; Romero-Sarria et al., 2008) or to results obtained with a high content of ethanol in the feed (vide infra). Absence or very low concentration of CO in products for composites promoted by oxides with a high Ce content (Table 2) implies that red-ox properties of promoters are also responsible for routes of ethanol transformation into carbon oxides (Erdőhelyi et al., 2006; Vargas et al., 2005). Since at high temperatures acetates are the only surface species detected by infra-red spectroscopy (Erdőhelyi et al., 2006), at short contact times CO_2 can be considered as primary product of their transformation. Since CH_4 was not observed in products, this transformation is not simple cracking usually accompanied by CH_4 formation, but should include interaction of ethoxide species with reactive hydroxyls or hydroxocarbonate species.

№	Sample	Products concentration. %		
		CO	CO_2	H_2
1	10% $Pr_{0.15}Sm_{0.15}Ce_{0.35}Zr_{0.35}O_2$+55% NiO+35%YSZ	0.1	0.4	1.1
2	80% $Pr_{0.15}Sm_{0.15}Ce_{0.35}Zr_{0.35}O_2$+10% NiO+10%YSZ	0.1	0.4	1.1
3	50%LaPrMnCr+30%NiO+20%YSZ	0.1	0.4	1.0
4	80%LaPrMnCr+10%NiO+10%YSZ	0.1	0.4	1.1
5	10%$Pr_{0.3}Ce_{0.35}Zr_{0.35}O_2$+90%NiO/YSZ	0.1	0.5	1.7
6	1%Ru/10%$Pr_{0.3}Ce_{0.35}Zr_{0.35}O_2$+90%NiO/YSZ	0.2	0.4	1.5
7	10%$Pr_{0.25}Ce_{0.5}Zr_{0.25}O_2$+90%NiO/YSZ	0	0.5	1.8
8	1%Ru/10%$Pr_{0.25}Ce_{0.5}Zr_{0.25}O_2$+90%NiO/YSZ	0	0.5	1.9
9	10%$Pr_{0.15}La_{0.15}Ce_{0.35}Zr_{0.35}O_2$+90%NiO/YSZ	0.1	0.3	1.3
10	1%Ru/10%$Pr_{0.15}La_{0.15}Ce_{0.35}Zr_{0.35}O_2$+90%NiO/YSZ	0.3	0.4	1.4
11	10%$Pr_{0.15}La_{0.15}Ce_{0.5}Zr_{0.2}O_2$+90%NiO/YSZ	0.1	0.3	1.1
12	Ru/10%$Pr_{0.15}La_{0.15}Ce_{0.5}Zr_{0.2}O_2$+90%NiO/YSZ	0.1	0.3	1.2
13	10%$Pr_{0.15}Sm_{0.15}Ce_{0.35}Zr_{0.35}O_2$+90%NiO/YSZ	0.1	0.3	2.0
14	Ru/10%$Pr_{0.15}Sm_{0.15}Ce_{0.35}Zr_{0.35}O_2$+90%NiO/YSZ	0	0.5	1.9
15	10%$Pr_{0.15}Sm_{0.15}Ce_{0.5}Zr_{0.2}O_2$+90%NiO/YSZ	0	0.5	1.9
16	Ru/10%$Pr_{0.15}Sm_{0.15}Ce_{0.5}Zr_{0.2}O_2$+90%NiO/YSZ	0	0.5	1.9

Table 2. Concentrations of products (H_2, CO and CO_2) in the ethanol steam reforming at 700 ^oC for different composites prepared by modified Pechini method (1-4) and by impregnation (combinatorial) rout (4-16). Contact time 0.036s, feed composition 0.5% C_2H_5OH + 2.5% H_2O in He.

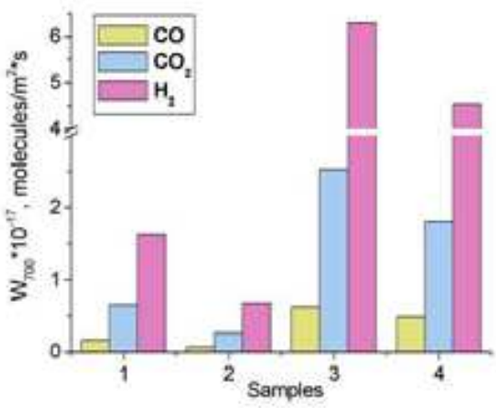

Fig. 20. Rates of products formation in ethanol steam reforming at 700 °C on nanocomposites. Contact time 36ms, feed 0.5% EtOH + 2.4%H_2O in He. 1-10%SmPrCeZr+55%NiO+35%YSZ, 2-80% SmPrCeZr +10%NiO +10%YSZ, 3-50%LaMnCrPr+30%NiO+20%YSZ, 4-80%LaMnCrPr +10%NiO+10%YSZ

Some variation of performance with nanocomposites composition and preparation route is worth commenting. For samples based on composite **III** prepared via successive impregnation, the lowest performance was demonstrated by nanocomposites containing $Pr_{0.15}La_{0.15}Ce_{0.7-x}Zr_xO_2$ (Table 2). This clearly correlates with the highest temperatures of H_2 TPR peaks for these samples (Sadykov et al., 2009b) reflecting their lower reducibility, and, hence, a lower mobility and reactivity of lattice oxygen due to stabilizing effect of a big basic La cation. Since in diluted ethanol+ water feeds the catalysts were tested after pretreatment in O_2, this correlation can be explained either by insufficient reduction of Ni in La-containing catalysts, or by a lower mobility and reactivity of surface hydroxyls/hydroxocarbonates bound with big La cation. The latter can result in the surface coking decreasing performance. Indeed, for nanocomposite promoted by $Pr_{0.15}La_{0.15}Ce_{0.5}Zr_{0.2}O_2$ with the lowest hydrogen concentration in products (Table 2), TPO oxidation after reaction revealed accumulation of up to 18 monolayers of carbonaceous deposits on the surface.

Effect of supporting Ru on promoted composite **III** strongly depends upon the composition of complex oxides (Table 2). For PrSmCeZr- promoted composites possessing a high activity, supporting Ru slightly decreases hydrogen yield. For composite promoted by $Pr_{0.15}Sm_{0.15}Ce_{0.35}Zr_{0.35}O_2$, co-promotion with Ru increases CO_2 yield but decreased CO and H_2 yield. Hence, at short contact times and in diluted feeds, water gas shift reaction is apparently not equilibrated.

When Ru was supported on less active composites promoted by La-containing oxides, another effects were observed: both hydrogen and CO_x yields were increased. While the increase of CO yield can be assigned to acceleration of reverse water gas shift reaction catalyzed by Ru particles weakly interacting with promoting fluorite-like oxides in these composites (vide supra), increase of hydrogen and CO_2 content in the feed suggests that the overall transformation of ethanol along the steam reforming route is accelerated as well, perhaps, due to decreasing the surface coking and/or accelerating other stages of intermediates (acetate etc) transformation into hydrogen and carbon oxides.

For SmPrCeZrO-promoted nanocomposites prepared via one-pot Pechini route (sample 1, Table 2) performance is lower than for nanocomposites of the same composition prepared via consecutive impregnation (sample 13, Table 2). This demonstrates that nanocomposite

microstructure affected by the preparation route plays important role in performance of these catalysts in steam reforming of ethanol.

The decrease of Ni content in nanocomposite from 55 to 10% only moderately decreased performance (Table 2), which can be explained by a higher dispersion of Ni (vide supra).

Nanocomposites promoted by LaPrMnCrO perovskite and prepared via Pechini route demonstrate a higher activity in ethanol steam reforming than catalysts promoted by doped ceria-zirconia oxides and prepared by the same method (Table 2, Fig. 20). Since the trend was usually reversed for CH_4 steam reforming, such a simple explanation as a higher dispersion of Ni more easily incorporated into the perovskite structure could be not sufficient. Perhaps, for ethanol steam reforming presence of red-ox cations such as Mn which can be involved in H_2O activation along with Ni (vide supra) can be important as well.

4.3 Catalytic performance of nanocomposites supported on structured substrates

For supporting thin layers of nanocomposites, Ni/YSZ anode plates, Ni-Al foam substrates as well as thin-foil or gauze Fechraloy substrates were used.

The Fecralloy gauze substrate (woven from the wires with diameter 0.2 mm and ca. 0.2 mm spacing) was first precovered by a thin (ca. 5–10 microns) corundum sublayer by blast dusting technique (Ulyanitskii et al., 2006) followed by washcoating with La-stabilized γ-Al_2O_3 (3.6 wt.%) from an appropriate suspension followed by calcination under air at 1100°C for 2 h. Before supporting active components, the gauze was cut into square pieces to be stacked with Ni-Al foam plates.

Composite powders synthesized via one-pot Pechini route (vide supra) were ultrasonically dispersed in isopropyl alcohol with addition of polyvinyl butyral as a binder to make a slurry. Thin layers of composites were supported on heat-conducting substrates using these slurries and slip casting or painting procedures followed by drying and calcination at 1100°C after each supporting step until loading of 4-7 wt.% was achieved. Ru or Pt were supported by the incipient wetness impregnation followed by drying and calcination under air at 800°C.

Catalytic performance of monolithic catalysts with nanocomposite active components on different substrates in the reaction of natural gas and ethanol steam reforming in concentrated feeds was studied in the stainless steel flow reactors equipped with external heating coils (Sadykov et al., 2010a) using a pilot-scale installation (feed rate up to 1 m^3/h). Water and ethanol were supplied by a pump and sprayed via a nozzle into a specially designed monolithic Fechralloy honeycomb evaporation/mixing unit heated by passing the electric current (Sadykov et al., 2009a). Reagents and products concentrations were analyzed by GC.

Fig. 21 compares methane conversions for different plate-like structural elements in stoichiometric steam/methane feed with supported layers of nanocomposite containing fluorite-like oxide promoter and Ru. While at temperatures below 550°C the initial Ni/YSZ anode substrate is not active, supporting composite layers on all substrates provides a reasonable activity in the low-temperature range. Activity of these layers on different substrates is comparable, which agrees with reasonably high intrinsic activity of nanocomposite active components (vide supra). This allows to use these structural elements for in-cell steam reforming of methane to provide an efficient heat management. A high activity of unpromoted Ni/YSZ anode platelet manufactured by the Research Center of Jülich (Germany) at temperatures exceeding 600°C is worth noting as well. In this case, as judged by the carbon balance, a slow coke accumulation in stoichiometric feed takes place which is to deactivate anode sooner or later.

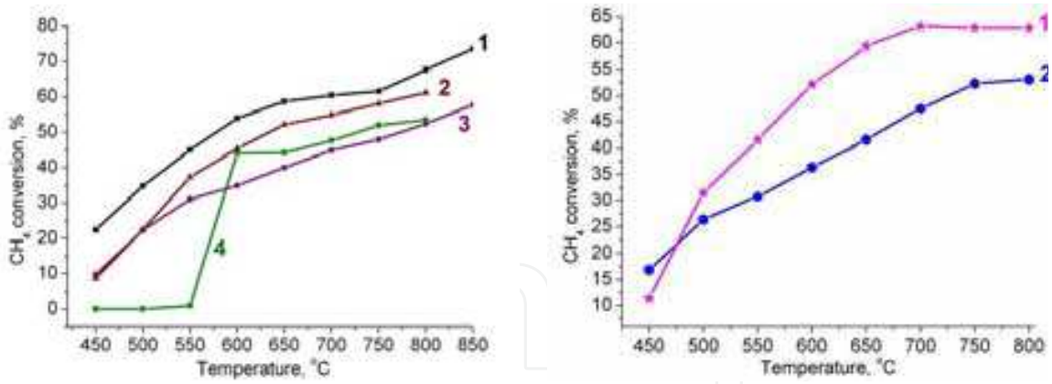

Fig. 21. Temperature dependence of CH_4 conversion on catalytic platelets of 1x2 cm^2 size. 8 % CH_4 +8% H_2O in He, contact time 25 ms. Left: 1%Ru/$Pr_{0.3}Ce_{0.35}Zr_{0.35}O_2$/Ni/YSZ layers on Ni/YSZ anode platelet (1) foam Ni-Al substrate (2) and Crofer interconnect (3). 4-unpromoted Ni/YSZ anode platelet. Right: 0.5%Ru/$La_{0.8}Pr_{0.2}Mn_{0.2}Cr_{0.8}O_3$/Ni/YSZ (1) and 0.5%Ru/$Pr_{0.3}Ce_{0.35}Zr_{0.35}O_2$ Ni/YSZ (2) layers on Ni/YSZ anode substrate.

When nanocomposite layers supported on different substrates contain as co-promoters Ru and perovskite-like oxide, performance is better than for combination of Ru and fluorite-like oxide (Fig. 21), following similar trend for powdered samples (vide supra). Combination of Pt with fluorite-like oxide as co-promoters in supported nanocomposite layers on different substrates also provides a high and stable activity in methane steam reforming even in feeds with higher (20%) concentration of methane close to realistic composition (Fig. 22).

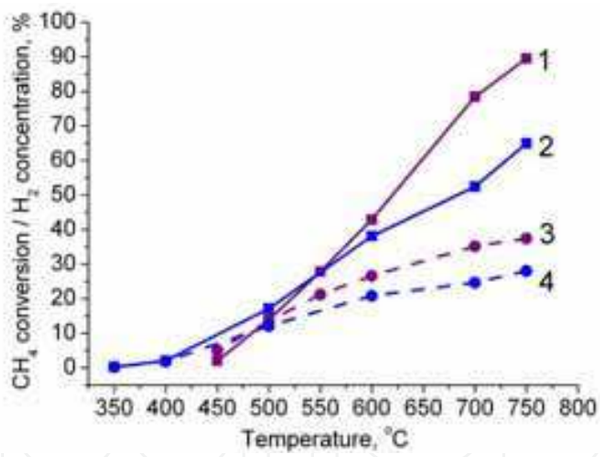

Fig. 22. Conversion of CH_4 (1,2) and H_2 concentration in converted dry feed (3,4) for CH_4 steam reforming on nanocomposite Pt/$Pr_{0.3}Ce_{0.35}Zr_{0.35}O_2$/Ni/YSZ layers supported on one side of Ni/YSZ anode platelet (1,3) or porous Ni-Al substrate (2,4). CH_4/H_20/Ar = 20/20/60. Contact time 25 ms.

As follows from both optical and SEM images after stability tests (Fig. 23), supported nanocomposite layer retains its integrity without any cracks or detachment from the underlying anode substrate despite transformation of NiO into Ni in composite as well as in the anode substrate in the reaction conditions. This is provided by a close composition of both substrate and supported layers ensuring matching of chemical and thermal coefficients of shrinkage/expansion. Developed porosity of supported layers helps to avoid diffusion limitations for rather fast CH_4 SR reaction.

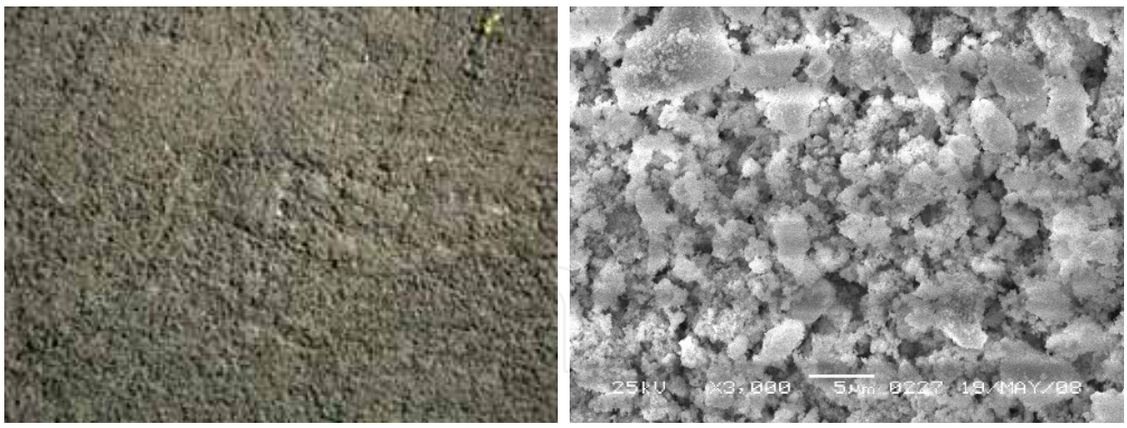

Fig. 23. Optical image (left, x50) and SEM image (right) of Ni/YSZ anode platelet with supported nanocomposite layer after stability tests.

In addition to the direct in-cell steam reforming of methane occurring on catalytically active anodes of SOFC, nanocomposite catalysts supported on heat-conducting substrates such as Crofer interconnects or foam Ni-Al alloy can be efficiently applied for so called indirect in-cell steam reforming of methane within the anode compartment of a stack (in fuel channels etc) (Dicks, 1998). In this case, the effect of the oxygen transfer across the cell under load is of much less importance, so selection of active components can be primary oriented on achieving the highest performance in feeds with steam/methane ratio close to stoichiometry and its stability.

For the indirect in-cell reforming of methane on separate structural elements comprised of nanocomposite active components supported on heat –conducting metal alloy substrates, the problem of thermal expansion compatibility with substrates is less crucial as compared with that for porous nanocomposite layers on anode platelets. Hence, content of Ni in active component can be decreased to improve its resistance to sintering and coking. On the other side, decreasing Ni content could decrease catalytic activity, especially in feeds with the water excess (vide supra).

Systematic studies of the effect of Ni content in nanocomposite active component on their performance revealed that the best compromise is achieved at Ni content in the nanocomposite with YSZ and complex promoting perovskite-like or fluorite-like oxides around 25% (NiO content in green nanocomposite 30 wt.%). As demonstrated in Fig. 24, in this case the active component provides required level of activity and on-stream stability when tested both as a fraction and as a porous layer supported onto foam Ni-Al substrate. Note that the temperature dependence of conversion is practically identical for the fraction and platelet. Hence, mass and heat transfer effects are indeed negligible for this type of substrate.

To check the effect of up-scaling the size of structured catalysts on their performance in the reaction of methane steam reforming, a package comprised of stacked foam platelets and gauzes was tested in concentrated natural gas/steam feeds.

For the stack comprised of either of 3 Ni-Al foam plates (Fig. 25) or 12 Ni-Al-foam plates and 11 sheets of Fecralloy gauzes loaded with $La_{0.8}Pr_{0.2}Mn_{0.2}Cr_{0.8}O_3$ + NiO + YSZ + Ru active component (Fig. 26), hydrogen concentration in the effluent was nearly identical at the same temperature and contact time. This means that heat and mass transfer does not affect strongly performance of these structured catalysts, which is rather good providing >45% H_2 in the effluent.

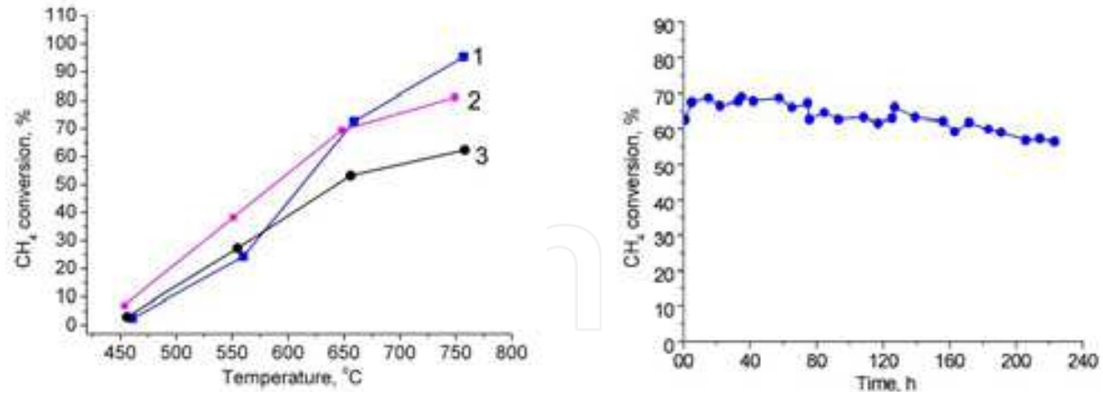

Fig. 24. Temperature dependence of CH_4 conversion (left) and its variation with time-on-stream at 600 °C (right) for 0.25 mm fraction of nanocomposite **V** +0.7Ru (1), and 1x2 cm^2 Ni-Al platelet with supported active component (2, 3). Loading 5.3 wt. % nanocomposite **V** +0.85 wt.% Ru (2) or 3.8 wt. % nanocomposite **V** +0.47 wt.% Ru (3). Contact time 10 ms for (1), 25 ms for (2, 3) and 50 ms for testing stability with time-on-stream. Feed composition 20% CH_4 +40% H_2O, Ar balance.

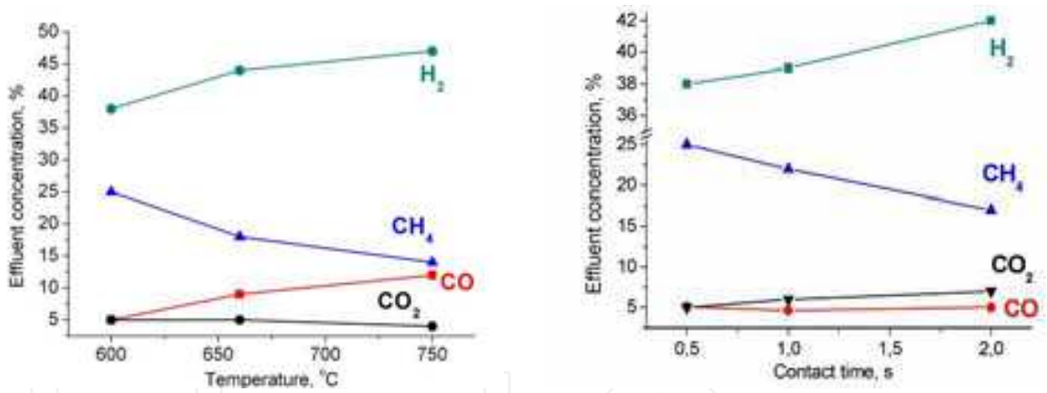

Fig. 25. Effect of temperature (left) and contact time (STP) at 600°C (right) on concentration of components in effluent for steam reforming of natural gas on stack of 3 plates 40x40x1 mm^3 each. Feed composition 35% of natural gas + 60% H_2O + 5%N_2; contact time 0.15 s at 600°C or 0.5 s at STP (left).

Tests for 100 h with start-up and shut-down of pilot installation each day (8 hours working time per day) confirmed stability of this level of H_2 content in effluent (Fig. 26).

The same package of 12 Ni-Al-foam plates and 11 sheets of Fecralloy gauzes loaded with $La_{0.8}Pr_{0.2}Mn_{0.2}Cr_{0.8}O_3$ + NiO + YSZ + Ru active component was used for oxysteam reforming of ethanol in pilot installation. In this process performance was also stable providing a high concentration of hydrogen (Fig. 27). The increase of steam excess in the feed helps to increase the hydrogen yield by increasing ethanol conversion as well as by decreasing content of such by-products as methane and ethylene.

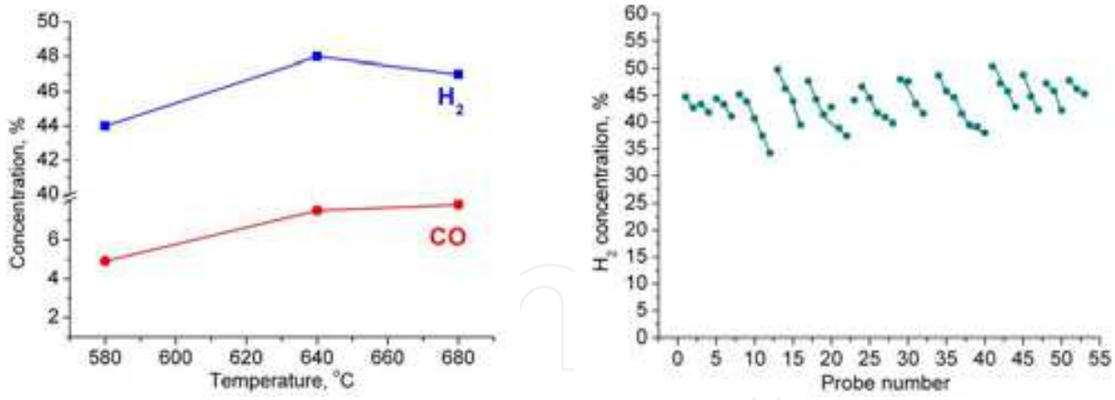

Fig. 26. Temperature dependence of H_2 and CO content in effluent (left) and stability tests at 630°C (right) for the reaction of natural gas (NG) steam reforming on a stack comprised of 12 Ni-Al-foam plates and 11 sheets of Fecralloy gauzes loaded with $La_{0.8}Pr_{0.2}Mn_{0.2}Cr_{0.8}O_3$ + NiO + YSZ + Ru (volume 34x34x34 mm^3). Feed 33% NG + H_2O (H_2O/C = 1.9) in Ar, contact time 0.15 s. Time between probes 2 h, package was cooled and warmed in steam each day.

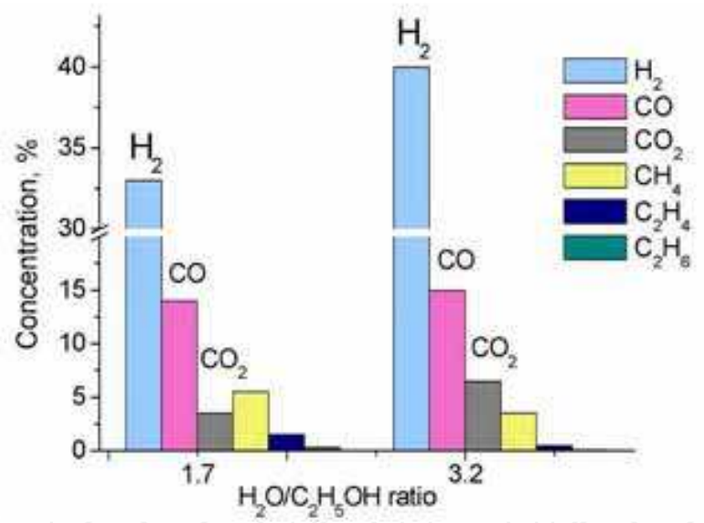

Fig. 27. Concentration of products in the effluent stream of ethanol oxysteam reforming on stack comprised of 12 Ni-Al-foam plates and 11 sheets of Fecralloy gauzes loaded with $La_{0.8}Pr_{0.2}Mn_{0.2}Cr_{0.8}O_3$ + NiO + YSZ + Ru (volume 34x34x34 mm^3). Feed composition: 5% O2+ H_2O +25% EtOH + N_2. T inlet 700°C, contact time 0.3 s.

5. Kinetic analysis of methane steam reforming on anode structural elements

The kinetics of the methane–steam reaction is based upon a 13-step mechanism of H_2; CO and CO_2 formation with three rate determining steps (Xu & Froment, 1989).
Three reversible macrosteps are as follows:

- *Steam reforming (SR)*

$$CH_4 + H_2O \leftrightarrow 3H_2 + CO \qquad \Delta_r H_{298\,K} = 206.2 \text{ kJ mol}^{-1} \tag{1}$$

- *Water-gas shift (WGS)*

$$CO + H_2O \leftrightarrow CO_2 + H_2 \qquad \Delta_r H_{298\,K} = -41.2 \text{ kJ mol}^{-1} \tag{2}$$

- *Complex shift reaction (SSR)*

$$CH_4 + 2H_2O \leftrightarrow 4H_2 + CO_2 \qquad \Delta_r H_{298\,K} = 165 \text{ kJ mol}^{-1} \tag{3}$$

Kinetic parameters of these steps were estimated by analyses of experimental data obtained in a slot-like reactor for the nanocomposite platelet with size 1x2 cm² loaded with 5.3% wt.% of nanocomposite 50%LaMnPr+30%NiO+20% YSZ promoted by 0.85 wt.% Ru. The power law rate equations for the reactions (1) - (3) were expressed in the general form:

$$R_{i,r}\left[kgmol \cdot m^{-1} \cdot s\right] = k_{f,r}\prod_{j=1}^{N_r}\left[C_{j,r}\right]^{\eta'_{j,r}} - k_{b,r}\prod_{j=1}^{N_r}\left[C_{j,r}\right]^{\eta''_{j,r}},$$

where Arhenius parameters for forward reaction rate constants are written in the form: $k_{f,r} = A_r T^{\alpha_r} \exp\left(-\frac{E_r}{RT}\right)$.

Here, N_r is number of chemical species in the overall molecular reaction r (SR, WGS, and SSR); $C_{j;r}$ is molar concentration of each reactant and product species j in reaction r (kgmol/m³); $\eta'_{j,r}$ is forward rate exponent for each reactant and product species j in reaction r, $\eta''_{j,r}$ is backward rate exponent for each reactant and product species j in reaction r. The backward rate constant for reaction r, $k_{b,r}$, were computed from the forward rate constant using the following relation: $k_{b,r} = \frac{k_{f,r}}{K_{eq,r}}$, where $K_{eq,r}$ is the equilibrium constants for the three main reactions (1)- (3) respectively:

$$K_{eq,SR}\left[atm^2\right] = \frac{p_{CO}p_{H_2}^3}{p_{CH_4}p_{H_2O}} = \exp\left(-\frac{\Delta G_{SR}}{RT}\right),$$

$$K_{eq,WGS}\left[atm^0\right] = \frac{p_{CO_2}p_{H_2}}{p_{CH_4}p_{H_2O}} = \exp\left(-\frac{\Delta G_{WGS}}{RT}\right),$$

$$K_{eq,SSR}\left[atm^2\right] = \frac{p_{CO}p_{H_2}^4}{p_{CH_4}p_{H_2O}^2} = \exp\left(-\frac{\Delta G_{SSR}}{RT}\right).$$

Respective values of effective kinetic parameters for the reactions (1) - (3) obtained by fitting the experimental data are given in Table 3.
The fixed conversion temperature dependences were analyzed with the developed rate equations (Table 3).

	$A_{f,r}$	α_r	$E_{f,r}, J/mol$
$r_{SR} = k_{f,SR} C_{CH_4} C_{H_2O}^2 - k_{b,SR} C_{H_2}^{0.25} C_{CO}$	4.5×10^4	-2.65	125000
$r_{WGS} = k_{f,WGS} C_{CO}^{0.85} C_{H_2O}^{0.65} - k_{b,WGS} C_{CO_2}$	2.4×10^2	0	42000
$r_{SSR} = k_{f,SSR} C_{CH_4} C_{H_2O}^{1.25} - k_{b,SSR} C_{H_2} C_{CO_2}$	38	0	81000

Table 3. Kinetic parameters of the rates of three basic macrosteps for the catalytic platelet loaded with nanocomposite active component.

To perform numerical experiments a steady state plug-flow reactor model describing the change of each reaction component along the catalytic platelet is written in the differential form:

$$\frac{d(uc_i)}{dl} = S_{sp} \sum_{j=1}^{3} \nu_{ij} r_j \tag{4}$$

Here, c_i is concentration of i-component in mol/m^3, u – superficial velocity of gas mixture through the reactor (m/s), S_{sp}– specific surface area, (m^{-1}), ν_{ij} -stoichiometric coefficients; r_j - reaction rate for the three global reactions (mol*m^{-2}*s^{-1}), expressed in the empirical form of the power law rate kinetics for the global reactions (1)-(3) as as $r_j = \frac{R_j}{S^*}$, where S*- active surface area (m^2/kg). A second-order Rozenbroke algorithm with an automatic choice of the integration interval was used to solve the set of equations. The Fortran computed code was developed to implement the described algorithm. The predictions based on the kinetic models with the parameters summarised in Table 3 were compared with the experimental data (Fig. 28). A good agreement demonstrates that the *power* law model is *able* to predict with certainty the reaction behavior within the temperature region 600-700^{o}C, which is of special interest in the case of in-cell methane reforming for intermediate temperature solid oxide fuel cells.

The same model was applied to analysis of experimental data on the natural gas steam reforming over stack comprised of three parallel Ni-Al platelets (50x50x1 mm) loaded with the same nanocomposite active component and separated by *1 mm gaps. In these experiments* operational temperature, the feed linear velocity and the steam-to-natural gas ratio were varied. A comparison of simulated and experimental data obtained for this stack has been performed by using kinetic parameters estimated for one small platelet (Table 3). The general quality of results obtained is illustrated in Figures 29 (a,b). A good agreement between experimental and simulated data demonstrates that the simple plug-flow reactor model is *able* to describe the reaction behaviour in the wide rage of the experimental conditions without taking into account heat and mass transfer effects due to high thermal conductivity and developed macroporosity of Ni-Al foam substrates.

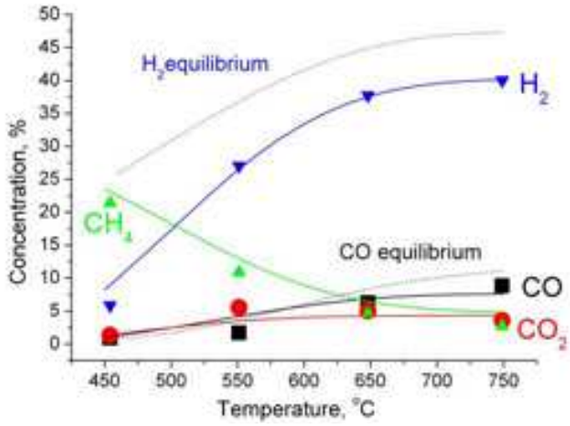

Fig. 28. Experimental and simulated (with kinetics – solid lines, thermodynamic predictions –dash lines) data (dry basis) on the effect of the temperature on the methane steam reforming reaction over Ni-Al foam platelet loaded with 5.3% wt.% of 50%LaMnPr+30%NiO+20% YSZ nanocomposite promoted by 0.85%Ru.

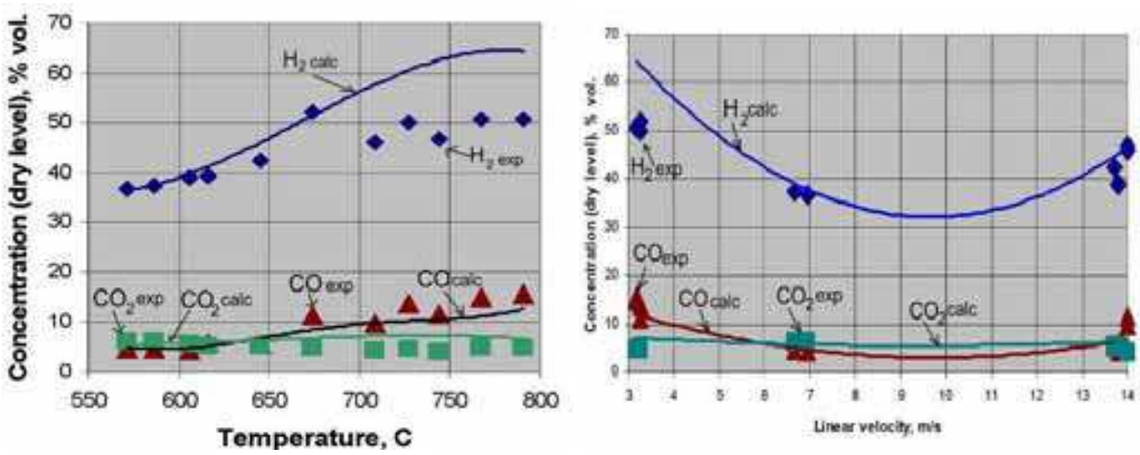

(a) (b)

Fig. 29. Effect of the operational temperature (a) and linear velocity of the feed gas (STP) (b) on the concentration of components in the product gas. Symbols – experimental data, lines – numerical experiments.

6. Results of catalytic element testing in planar SOFC

The cell tests were performed in the Energy Research Center (Petten, Netherlands) in a test bench with an alumina housing for 5x5 cm² cells (Ouweltjes et al., 2008).

Fuel cells were assembled in configuration Pt grid/LSC/20GCO/8YSZ/Ni-YSZ anode substrate/Ni-Al foam catalytic plate/Ni grid. Here platinum grid was used for cathode current collection, LSC is cathode La-Sr-cobaltite layer, 20GDC- $Ce_{0.8}Gd_{0.2}O_{2-y}$ interlayer between cathode and a thin layer of YSZ supported on a planar Ni-YSZ anode substrate. Nickel mesh as anode current collector was pressed to Ni-Al catalytic plate, so current was passed through it. A stream of $CH_4 + H_2O$ feed ($H_2O/CH_4 = 2$) or hymidified H_2 was passed along the catalytic plate loaded with 5 wt.% of nanocomposite 50% LaMnCrPr + 30%NiO +

20%YSZ promoted by 1.3 wt.% Ru. Air stream was used as oxidant from the cathode side. Electrochemical characterisation was performed by V/I curves and impedance spectroscopy with a Solartron 1255/1287 set-up.

At 600 ^{o}C and 700 mV the area specific resistance (ASR) was estimated to be 0.77 Ohm cm^2 without any contribution of catalyst to R_{ohm}, which meets target of operation for intermediate temperature solid oxide fuel cells.

Fig. 30 presents I- V characteristics of this cell with CH_4 or H_2 as a fuel. As follows from these data, at 800 ^{o}C cell performance for both types of fuels is comparable, which demonstrates a high efficiency of planar catalytic element in steam reforming of methane. Power density up to 350-850 mW/cm^2 is achieved in 600-800 ^{o}C range, which is promising for the practical application. At CH_4 flow 90 ml/min and 600 ^{o}C CH_4 conversion increases from 47 to 55% with increasing current from 0 to 4A. This conversion is rather close to values obtained at this temperature for single platelet with this active component (Fig. 21).

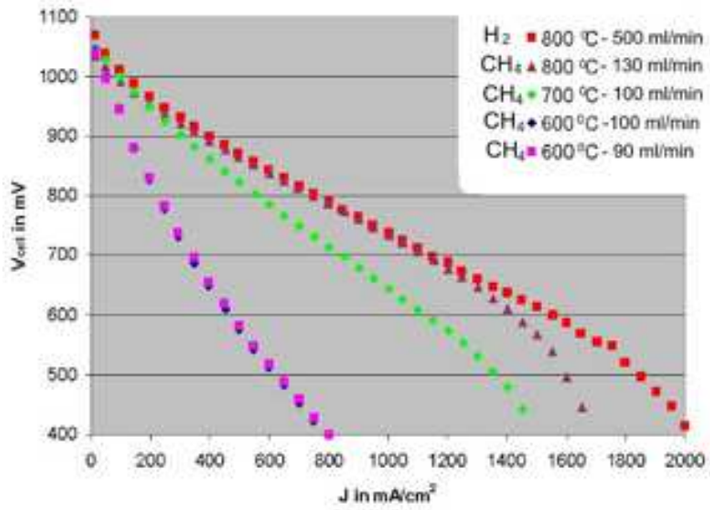

Fig. 30. I- V characteristics of cell equipped with Ni-Al foam-supported nanocomposite catalyst using CH_4 or H_2 as a fuel.

7. Conclusion

Nanocomposite materials developed in this work based upon Ni and doped zirconia electrolyte allow to provide efficient and stable in-cell steam reforming of methane and ethanol required for IT SOFC as well as design of monolithic catalysts of transformation of biofuels into syngas. This is provided by optimization of their composition and preparation procedures ensuring developed interfaces between components activating fuel molecules (Ni, Ni-Pt/Ru alloys) and water molecules (complex oxides with perovskite and fluorite structures). Performance of best compositions supported as porous strongly adhering layers on anode cermets platelets, FeCralloy gauzes and porous Ni-Al foam substrates was estimated as well and demonstrated to be high and stable to meet target of internal reforming of fuels in the intermediate temperature solid oxide fuel cells. No cracking or detachment of layers after reaction was observed. Analysis of methane reforming kinetics catalyzed by structured catalytic elements with supported nanocomposite layers has been carried out. Performance of catalytic plates in IR mode of ECN cell meets target of design of

solid oxide fuel cells with internal reforming of methane by area specific resistance, activity and power density.

8. Acknowledgements

The authors gratefully acknowledge the financial support from NATO SFP 980878, SOFC 600 FP6 EC Project, Integration Project 57 of SB RAS- NAN Belarus, Project 57 of RAS Presidium Program No. 27 and RFBR-ofi_m 09-03-12317 Project.

9. References

Ana, S., Lu, C., Worrell, L., W., J. Gorte, R., M. Vohs, (2004), "Characterization of Cu–CeO_2 Direct Hydrocarbon Anodes in a Solid Oxide Fuel Cell with Lanthanum Gallate Electrolyte", *Solid State Ionics*, 175, 135–138, ISSN 0167-2738.

Asadullah, M, Ito, S., Kunimori, K. Yamada, M. Tomishige, (2002), "Biomass Gasification to Hydrogen and Syngas at Low Temperature: Novel Catalytic System Using Fluidized-Bed Reactor" K., *J Catal*. 208, 2, 255-259, ISSN 0021-9517

Atkinson, A., Barnett, S., Gorte, R., Irvine, J., Mcevoy, A., Mogensen, M., C. Singhal, S., Vohs, J., (2004), "Advanced Anodes for High-Temperature Fuel Cells", *Nature*, 3, 17–27, ISSN 0028-0836

Bebelis, S., Neophytides, S., Kotsionopoulos, N., Triantafyllopoulos, N., Colomer, M., Jurado, J., (2006), "Methane Oxidation on Composite Ruthenium Electrodes in YSZ Cells", *Solid State Ionics*, 177, 2087 –2091, ISSN 0167-2738

Bernal, S. Calvino, J.J. Gatica, J.M. Cartes, C.L. Pintado, J.M, (2002),"Chemical and Nanostructural Aspects of the Preparation and Characterisation of Ceria and Ceria-based Mixed Oxide-Supported Metal Catalysts". in: Catalysis by Ceria and Related Materials; Trovarelli, A.; Ed.; Catalytic Science Series; Imperial College Press: London, UK, 2002. Vol. 2, pp 85-168, ISBN 1-86094-299-7

Boldyrev, V. V., Bulens, M., and Delmon, B. (1979), "The Control of the Reactivity of Solids. A Critical Survey of the Factors that Influence the Reactivity of Solids, with Special Emphasis on the Control of the Chemical Processes in Relation to Practical Application." *Stud. Surf. Sci. Catal.*, 2, p. 215. ISBN 9870444418005

Breen, P., Burch, R., Coleman, H.M., (2002), "Metal-catalysed steam reforming of ethanol in the production of hydrogen for fuel cell applications", *Appl. Catal. B*: Environ. 39, 1, 65-74, ISSN 0926-3373

Dicks, A., (1998), "Advances in Catalysts for Internal Reforming in High Temperature Fuel Cells", *Journal of Power Sources*, 71, 111–122. ISSN 0378-7753

Domine M. E., Iojoiu E. E., Davidian T., Guilhaume N., Mirodatos C., (2008), "Hydrogen production from biomass-derived oil over monolithic Pt- and Rh-based catalysts using steam reforming and sequential cracking processes", *Catalysis Today* 133–135, 565–573, ISSN 0920-5861

Dongare, M., Dongare, A., Tare, V., Kemnitz, E, 2002, "Synthesis and Characterization of Copper-Stabilized Zirconia as an Anode Material for SOFC", *Solid State Ionics*, 152–153, 455– 462, ISSN 0167-2738

Erdőhelyi, A., Raskó, J., Kecskés, T., Tóth, M., Dömök, M., Baán, K., (2006), "Hydrogen formation in ethanol reforming on supported noble metal catalysts" *Catal. Today*, 116., 3., 367-376, ISSN 0920-5861

Fatsikostas, A.N., Kondarides, D.I., Verykios, X.E., (2002), "Production of hydrogen for fuel cells by reformation of biomass-derived ethanol", *Catal. Today*, 75, 1-4, 145-155, ISSN 0920-5861

Frolova, E., Ivanovskaya, M., Sadykov, V., Alikina, G., Lukashevich, A., (2006), "Properties of Ce-Zr-La-O nano-system with ruthenium modified surface", *Progress in Solid State Chemistry*, 33, 2-4., 254-262, ISSN 0079-6786

Haryanto, A., Fernando, S., Murali, N., Adhikari, S., (2005) "Current Status of Hydrogen Production Techniques by Steam Reforming of Ethanol: A Review", *Energy & Fuels*, 19, 5, 2098-2106. ISSN 0887-0624

Hosokawa, S., Kanai, H., Utani, K., Taniguchi, Y., Saito, Y., Imamura, S., (2003) "State of Ru on CeO_2 and its catalytic activity in the wet oxidation of acetic acid", *Appl. Catal. B: Environ.*, 45, 3, 181-187. ISSN 0926-3373

Ishihara, T., Shibayama, T., Nishiguchi, H., Takita, Y., (2000), "Nickel–Gd-doped CeO_2 Cermet Anode for Intermediate Temperature Operating Solid Oxide Fuel Cells using LaGaO -Based Perovskite Electrolyte", *Solid State Ionics*, 132, 3-4, 209–216. ISSN 0167-2738

Jamsak, W., Assabumrungrat, S., Douglas, P.L., Laosiripojana, N., Suwanwarangkul, R., Charojrochkul, S., Croiset, E., (2007), "Performance of ethanol-fuelled solid oxide fuel cells: Proton and oxygen ion conductors", *Chem. Eng. J.*, 133, 1-3, 187-194. ISSN 1385-8947

Kharton, V., Yaremchenko, A., Valente, A., Frolova, E., Ivanovskaya, M., Frade, J., Marques, F., Rocha, J., (2006), "Methane Oxidation over SOFC Anodes with Nanocrystalline Ceria-based Phases", *Solid State Ionics*, 177, 19-24, 2179 –2183. ISSN 0167-2738

de Lima, S., O. da Cruz, I., Jacobs, G., Davis, B.H., Mattos, L.V., Noronha F.,B., (2008), "Steam reforming, partial oxidation, and oxidative steam reforming of ethanol over $Pt/CeZrO_2$ catalyst", *J Catal.*, 257, 2, 356–368. ISSN 0021-9517

Marina, O., Bagger, C., Primdal, S., Mogensen, M., 1999, "A Solid Oxide Fuel Cell with a Gadolinia-Doped Ceria Anode: Preparation and Performance", *Solid State Ionics*, 123, 1-4, 199-208. ISSN 0167-2738

Matsumura, Y., Nakamori, T., (2004), "Steam reforming of methane over nickel catalysts at low reaction temperature" *Appl. Catal. A: General*, 258, 1, 107-114. ISSN 0926-860X

Montoya, J.A., Romero-Pascual, E., Gimon, C., Del Angel, P., Monzon, A., (2000), "Methane reforming with CO_2 over Ni/ZrO_2–CeO_2 catalysts prepared by sol–gel" *Catal. Today*, 63, 1, 71-85. ISSN 0920-5861

Mezentseva, N., Alikina, G., Bunina, R., Pelipenko, V., Ishchenko, A., Smirnova, A., Smorygo, O., Sadykov, V., (2010), „Steam Reforming of Methane on Ru and Pt Promoted Nanocomposites for SOFC Anodes", *Mater. Res. Soc. Symp. Proc.* 1217, Y03-11.1-6. ISBN 978-1-60511-190-2

Ouweltjes, J. P. van Berkel, F., Rietveld, B., (2008), "Development and Evaluation of Redox Tolerant Anodes", Proc. 8th European SOFC Forum, 2008, Lucerne, Switzerland, 30 June – 4 July 2008, A0504.1-6 (CD).

Pavlova, S., Sazonova, N., Sadykov, V., Alikina, G., Lukashevich, A., Gubanova, E., Bunina, R., (2007), „Study of synthesis gas production over structured catalysts based on $LaNi(Pt)O_x$- and $Pt(LaPt)$-CeO_2-ZrO_2 supported on corundum", *Stud. Surf. Sci. Catal.*, 167, 343-348. ISBN 10 0-444-53078-9

Peña-Martínez, J., Marrero-López, D., Ruiz-Morales, J., Savaniu, C., Núñez, P., and Irvine, J., (2006), "Anodic Performance and Intermediate Temperature Fuel Cell Testing of $La_{0.75}Sr_{0.25}Cr_{0.5}Mn_{0.5}O_{3-\delta}$ at Lanthanum Gallate Electrolytes", *Chem. Mater.*, 18, 1001-1006. ISSN 0897-4756

Plint, S., Connor, P., Tao, Sh., Irvine, J., (2006), "Electronic Transport in the Novel SOFC Anode Material $La_{1-x}Sr_xCr_{0.5}Mn_{0.5}O_{3\pm\delta}$", *Solid State Ionics*, 177, 3-4, 2005–2008. ISSN 0167-2738

Primdahl, S., Mogensen, M., 2002, "Mixed Conductor Anodes: Ni as Electrocatalyst for Hydrogen Conversion", *Solid State Ionics*, 152– 153, 597-608. ISSN 0167-2738

Resini, C., Concepcion, M., Delgado, H., Presto, S., Alemany, L.J., Riani, P., Marazza, R., Ramis, G., Busca, G., (2008) "Yttria-stabilized zirconia (YSZ) supported Ni–Co alloys (precursor of SOFC anodes) as catalysts for the steam reforming of ethanol", *Int. J Hydrogen Energy*, 33, 3728 – 3735. ISSN 0360-3199

Romero-Sarria, F., Vargas, J. C., Roger, A.-C., Kiennemann, A., (2008), "Hydrogen production by steam reforming of ethanol: Study of mixed oxide catalysts $Ce_2Zr_{1.5}Me_{0.5}O_8$: Comparison of Ni/Co and effect of Rh" *Catal. Today*, 133-135, 149-153. ISSN 0920-5861

Sadovskaya, E.M., Ivanova Y.A., Pinaeva L.G., Grasso G., Kuznetsova T.G., van Veen A., Sadykov V.A., Mirodatos C., (2007), "Kinetics of Oxygen Exchange over CeO_2−ZrO_2 Fluorite-Based Catalysts", *J Phys. Chem. A*, 111, 20, 4498-4505, ISSN 1089-5639

Sadykov, V., Pavlova, S., Bunina, R., Alikina, G., Tikhov, S., Kuznetsova, T., Frolova, Yu., Lukashevich, A., Snegurenko, O., Sazonova, N., Kazantseva, E., Dyatlova, Yu., Usol'tsev, V., Zolotarskii, I., Bobrova, L., Kuz'min, V., Gogin, L., Vostrikov, Z., Potapova, Yu., Muzykantov, V., Paukshtis, E., Burgina, E., Rogov, V., Sobyanin, V., and Parmon, V., (2005a), "Selective Oxidation of Hydrocarbons into Synthesis Gas at Short Contact Times: Design of Monolith Catalysts and Main Process Parameters", *Kinetics and Catalysis*, 46, 2, 227–250. ISSN 0023-1584

Sadykov, V., Borchert, Yu., Alikina, G., Lukashevich, A., Bunina, R., Zabolotnaya, G., Mezentseva, N., Moroz, E., Zaikovskii, V., Zyuzin, D., Uvarov, N., Zyryanov, V., Orlovskaya, N., (2005b), "One-Pot Synthesis of Mixed Ionic-Electronic Conducting Nanocomposites Comprised of Fluorite-Like and Perovskite-Like Phases as Catalytic Materials for SOFC", *Mater. Res. Soc. Symp. Proc.*, 900E, O10.08.1-6. ISSN 9781558998551

Sadykov, V.A., Kuznetsova, T. G., Frolova, Yu. V., Alikina, G. M., Lukashevich, A. I., Rogov V.A., Muzykantov V. S., Pinaeva, L.G., Sadovskaya, E. M., Ivanova, Yu. A., Paukshtis, E. A., Mezentseva, N.V., Batuev, L.Ch., Parmon, V.N., Neophytides, S., Kemnitz, E., Scheurell, K., Mirodatos, C., van Veen, A.C., (2006a) „Fuel-rich methane combustion: role of the Pt dispersion and oxygen mobility in a fluorite-like complex oxide support", *Catalysis Today*, 117, 4, 475–483. ISSN 0920-5861

Sadykov, V., Frolova- Borchert, Yu., Mezentseva, N., Alikina, G., Lukashevich, A., Paukshtis, E., Muzykantov, V., Batuev, L., Kuznetsova, T., Moroz, E., Zyuzin, D., Kol'ko, V., Burgina, E., Kriventsov, V., Kochubei, D., Kemnitz, E., Scheurell, K., (2006b), "Nanocrystalline Catalysts Based on CeO_2-ZrO_2 Doped by Praseodymium or Gadolinium: Synthesis and Properties", *Mater. Res. Soc. Symp. Proc.*, 900E, O10-04.1-6. ISSN 9781558998551

Sadykov, V., Mezentseva, N., Bunina, R., Alikina, G., Lukashevich, A., Rogov, V., Moroz, E., Zaikovskii, V., Ishchenko, A., Bobrenok, O., Smirnova, A., Irvine, J., and Vasylyev, O., (2006c), "Design of Anodes for IT SOFC: Effect of Complex Oxide Promoters and Pd on Activity and Stability in Methane Steam Reforming of Ni/YSZ (ScSZ) Cermets", *Mater. Res. Soc. Symp. Proc*, 972, AA03-06. 1-6. ISBN 978-1-55899-929-9

Sadykov, V. A., Kuznetsova, T. G., Alikina, G. M., Frolova, Yu. V., Lukashevich, A. I., Muzykantov, V. S., Rogov, V. A., Batuev, L.Ch., Kriventsov, V. V., Kochubei, D. I., Moroz, E. M., Zyuzin, D. A., Paukshtis, E. A., Burgina, E. B., Trukhan, S.N., Ivanov, V.P., Pinaeva, L.G., Ivanova, Yu. A., Kostrovskii, V.G., Neophytides, S., Kemnitz, E., Scheurel, K., Mirodatos, C., (2007a) CERIA-BASED FLUORITE-LIKE OXIDE SOLID SOLUTIONS PROMOTED BY PRECIOUS METALS AS CATALYSTS OF METHANE TRANSFORMATION INTO SYNGAS. In Book: *New Topics in Catalysis Research* (Ed. D.K. McReynolds), 97-196, Chapter 5, Nova Science Publishers, NY, USA, ISBN 10 1-60021-286-7

Sadykov, V., Pavlova, S., Vostrikov, Z., Sazonova, N., Gubanova, E., Bunina, R., Alikina, G., Lukashevich, A., Pinaeva, L., Gogin, L., Pokrovskaya, S., Skomorokhov, V., Shigarov, A., Mirodatos, C., van Veen, A., Khristolyubov, A., Ulyanitskii, V., (2007b), „Performance of monolithic catalysts with complex active component in partial oxidation of methane into syngas: experimental studies and modeling", *Stud. Surf. Sci. Catal.* 167, 361-366. ISBN 10 0-444-53078-9

Sadykov, V., Mezentseva, N., Alikina, G., Lukashevich, A., Muzykantov, V., Kuznetsova, T., Batuev, L., Fedotov, M., Moroz, E., Zyuzin, D., Kolko, V., Kriventsov, V., Ivanov, V., Boronin, A., Pazhetnov, E., Zaikovskii, V., Ishchenko, A., Rogov, V., Ross, J., Kemnitz, E., (2007c), "Nanocrystalline Doped Ceria-Zirconia Fluorite-Like Solid Solutions Promoted by Pt: Structure, Surface Properties and Catalytic Performance in Syngas Generation", *Mater. Res. Soc. Symp. Proc.* 988, QQ06-04.1-6. ISBN 9781604234336

Sadykov, V., Kriventsov, V., Moroz, E., Borchert, Yu., Zyuzin, D., Kol'ko, V., Kuznetsova, T., Ivanov, V., Boronin, A., Mezentseva, N., Burgina, E., Ross, J., (2007d), "Ceria-Zirconia Nanoparticles Doped with La or Gd: Effect of the Doping Cation on the Real Structure", *Solid State Phenomena,* 128, 81-88. ISSN 1012-0394

Sadykov, V., Mezentseva, N., Alikina, G., Lukashevich, A., Borchert, Yu., Kuznetsova, T., Ivanov, V., Trukhan, S., Paukshtis, E., Muzykantov, V., Kriventsov, V., Rogov, V., Ross, J., Kemnitz, E., Sheurell, K., (2007e), "Pt-Supported Nanocrystalline Ceria-Zirconia Doped with La, Pr or Gd: Factors Controlling Syngas Generation in Partial Oxidation/Autothermal Reforming of Methane or Oxygenates", *Solid State Phenomena,* 128, 239-248. ISSN 1012-0394

Sadykov, V., Mezentseva, N., Pelipenko, V., Smorygo, O., Rietveld, B. (2008a) „Anode materials for IT SOFC based on NiO/YSZ doped with complex oxides and promoted by Pt, Ru or Pd: properties and catalytic activity in the steam reforming of CH_4", Proceedings of 8th European SOFC Forum, pp. A0526 : 1-6 Lucerne/Switzerland 30 June – 4 July 2008 (CD).

Sadykov, V., Mezentseva, N., Bunina, R., Alikina, G., Lukashevich, A., Kharlamova, T., Rogov, V., Zaikovskii, V., Ischenko, A., Krieger, T., Bobrenok, O., Smirnova, A., Irvine, J., Vasylyev, O., (2008b), "Effect of Complex Oxide Promoters and Pd on Activity and Stability of Ni/YSZ (ScSZ) Cermets as Anodes for IT SOFC", *Catalysis Today* 131, 1-4, 226–237. ISSN 0920-5861

Sadykov, V., Bobrova, L., Pavlova, S., Simagina, V., Makarshin, L., Parmon, V., Ross, J. R. H., Mirodatos, C., Van Veen, A. C., Khristolyubov, A. P., (2009a) Syngas Generation from Hydrocarbons and Oxygenates with Structured Catalysts, Chapter in Book "*Syngas: Production Methods, Post Treatment and Economics*" (A. Kurucz and I. Bencik, Eds.), pp. 53-140, Nova Science Publishers, Inc.,, New York, 2009. ISBN 978-1-60741-841-2

Sadykov, V., Mezentseva, N., Alikina, G., Bunina, R., Rogov, V., Krieger, T., Belochapkine, S., Ross J., (2009b), „Composite catalytic materials for steam reforming of methane and oxygenates: Combinatorial synthesis, characterization and performance", *Catal. Today*, 145, 1-2, 127–137. ISSN 0920-5861

Sadykov, V., Mezentseva, N., Alikina, G., Bunina, R., Pelipenko, V., Lukashevich, A., Tikhov, S., Usoltsev, V., Vostrikov, Z., Bobrenok, O., Smirnova, A., Ross, J., Smorygo, O., Rietveld, B., (2009c), „Nanocomposite catalysts for internal steam reforming of methane and biofuels in solid oxide fuel cells: Design and performance", *Catal. Today*, 146, 1-2, 132–140. ISSN 0920-5861

Sadykov, V., Mezentseva, N., Muzykantov, V., Efremov, D., Gubanova, E., Sazonova, N., Bobin, A., Paukshtis, E., Ishchenko, A., Voronin, V., Ross, J., Mirodatos, C., van Veen, A., (2009d) "Real Structure-Oxygen Mobility Relationship in Nanocrystalline Doped Ceria-Zirconia Fluorite-Like Solid Solutions Promoted by Pt", *Mater. Res. Soc. Symp. Proc.*, 1122., 1122-O05-03. ISSN 9781615677627

Sadykov, V., Sobyanin, V., Mezentseva, N., Alikina, G., Vostrikov, Z., Fedorova , Y., Pelipenko, V., Usoltsev, V., Tikhov, S., Salanov, A., Bobrova, L., Beloshapkin, S., Ross, J., Smorygo, O., Ulyanitskii, V., Rudnev, V., (2010a), „Transformation of CH_4 and liquid fuels into syngas on monolithic catalysts", *Fuel*, 89, 1230–1240. ISSN 0016-2361

Sadykov, V., Mezentseva, N., Bunina, R., Alikina, G., Lukashevich, A., Zaikovskii, V., Bobrenok, O., Irvine, J., Vasylyev O., Smirnova, A., (2010b) „Design of Anode Materials for IT SOFC: Effect of Complex Oxide Promoters and Pt Group Metals on Activity and Stability in Methane Steam Reforming of Ni/YSZ (ScSZ) Cermets", *J Fuel Cell Sci. Technol.*, 7, 1, 011005. 1-6. ISSN 1550-624X

Sadykov, V., Muzykantov, V., Bobin, A., Mezentseva, N., Alikina, G., Sazonova, N., Sadovskaya, E., Gubanova, L., Lukashevich, A., Mirodatos, C., (2010c), "Oxygen mobility of Pt-promoted doped CeO_2–ZrO_2 solid solutions: Characterization and effect on catalytic performance in syngas generation by fuels oxidation/reforming", *Catal. Today*, doi:10.1016/j.cattod.2010.03.064 ISSN 0920-5861

Sanchez-Sanchez, M.C., Navarro, R.M., Fierro, J.L.G., (2007), "Ethanol steam reforming over Ni/La–Al_2O_3 catalysts: Influence of lanthanum loading", *Catal. Today*, 129, 3-4, 336-345. ISSN 0920-5861

Sfeir, J., Buffat, P., Möckli, P., Xanthopoulos, N., Vasquez, R., Mathgieu, H., Herle, J., Thampi, K., (2001), "Lanthanum Chromite Based Catalysts for Oxidation of Methane Directly on SOFC Anodes", *J Catal.* 202, 2, 229-244. ISSN 0021-9517

Sauvet, A., Irvine, J., (2004), "Catalytic Activity for Steam Methane Reforming and Physical Characterisation of $La_{1-x}Sr_xCr_{1-y}Ni_yO_{3-\delta}$", *Solid State Ionics*, 167, 1 –8. ISSN 0167-2738

Smirnova, A., Sadykov, V., Muzykantov, V., Mezentseva, N., Ivanov, V., Zaikovskii, V., Ishchenko, A., Sammes, N., Vasylyev, O., Kilner, J., Irvine, J., Vereschak, V., Kosacki, I., Uvarov, N., and Zyryanov, V., (2007), "Scandia –Stabilized Zirconia: Effect of Dopants on Surface/Grain Boundary Segregation and Transport Properties", *Mater. Res. Soc. Symp. Proc.*, 972, AA10-05.1-6 ISBN 978-1-55899-929-9

Smorygo, O., Mikutski, V., Marukovich, A., Vialiuha, Y., Ilyushchanka, A., Mezentseva, N., Alikina, G., Vostrikov, Z., Fedorova, Y., Pelipenko, V., Bunina, R., Sadykov, V., (2009), „Structured catalyst supports and catalysts for the methane indirect internal steam reforming in the intermediate temperature SOFC", *Int. J Hydr. Energy*, 34, 9505 – 9514. ISSN 0360-3199

Souza, M.M.V.M., Schmal, M., (2003) "Combination of carbon dioxide reforming and partial oxidation of methane over supported platinum catalysts", *Appl. Catal. A: Gen.*, 255, 1, 83-92. ISSN 0926-860X

Srinivas, D., Satyanarayana, C.V.V., Potdar, H.S., Ratnasamy, P., (2003), "Structural studies on NiO-CeO_2-ZrO_2 catalysts for steam reforming of ethanol", *Appl. Catal. A: General*, 246, 2, 323–334. ISSN 0926-860X

Suzuki, M., Sasaki, H., Otoshi, S., Kajimura, A., and Ippommatsu, M., 1993, "High Power Density Solid Oxide Electrolyte Fuel Cells using Ru/Y_20_3 Stabilized Zirconia Cermet Anodes", *Solid State lonics*, 62, 1-2, 125-130. ISSN 0167-2738

Takeguchi, T., Kikuchi, R., Yano, T., Eguchi, K., Murata, K., (2003), "Effect of Precious Metal Addition to Ni-YSZ Cermet on Reforming of CH_4 and Electrochemical Activity as SOFC Anode", *Catal. Today*, 84, 3-4, 217-222. ISSN 0920-5861

Ulyanitskii, V., Shterzer, A., Zlobin, S., Matrenin, V., Schipanov, I. Serykh, S., Stikhin, A., Tretyakova, L., Sadykov, V., Pavlova, S., Tikhov, S., Kuzmin, V., (2006), "Blast dusting of refractory protective layers for solving the problems of hydrogen energetics", *Alternative Energetics and Ecology*, 9, 137-144. ISSN 1608-8298

Vargas, J. C., Libs, S., Roger, A.-C., Kiennemann, A., (2005), "Study of Ce-Zr-Co fluorite-type oxide as catalysts for hydrogen production by steam reforming of bioethanol" *Catal. Today*, 107–108, 417-425. ISSN 0920-5861

Vernoux, P., Guindet, J., Kleitz, M, (1998), "Gradual Internal Methane Reforming in Intermediate-Temperature Solid-Oxide Fuel Cell", *J Electrochem. Soc.*, 145, 10, 3487-3492. ISSN 0013-4651

Wan, J., Goodenough, J., (2005), "Solid Oxide Fuel Cell with a $La_{0.75}Sr_{0.25}Cr_{0.5}Mn_{0.5}O_{3-\delta}$ Anode and an LSGM Electrolyte", *Electrochem. Soc. Proc.*, 07, 429-434.

Wincewicz, K., Cooper, J., (2005), "Taxonomies of SOFC Material and Manufacturing Alternatives", *Journal of Power Sources*, 140, 280–296. ISSN 0378-7753

Wei, J., Iglesia, E., (2004), "Mechanism and Site Requirements for Activation and Chemical Conversion of Methane on Supported Pt Clusters and Turnover Rate Comparisons among Noble Metals", *J Phys. Chem. B*, 108, 13, 4094-4103. ISSN 1520-6106

Xia, C., Liu, M., (2002), "Microstructures, Conductivities, and Electrochemical Properties of $Ce_{0.9}Gd_{0.1}O_2$ and GDC–Ni Anodes for Low-Temperature SOFCs", *Solid State Ionics*, 152– 153, 423– 430. ISSN 0167-2738

Xu, J., Froment, G. F.,(1989), "Methane steam reforming, methanation and water-gas shift. I. Intrinsic kinetics", *AIChE J* 35, 1, 88-96, ISSN 0001-1541

Yan, A., Liu, B., Tu, B., Dong, Y., Cheng, M., Song, Sh., Tsiakaras, P., (2007) " A Temperature-Programmed-Reduction Study on $La_{1-x}Sr_xCrO_3$ and Surface-Ruthenium-Modified $La_{1-x}Sr_xCrO_3$ ", *J Fuel Cell Sci. Technol.*, 4, 79-83. ISSN 1550-624X

Yaseneva, P., Pavlova, S., Sadykov, V., Alikina, G., Lukashevich, A., Rogov, V., Belochapkine, S., Ross J., (2008) "Combinatorial approach to the preparation and characterization of catalysts for biomass steam reforming into syngas.", *Cat. Today*, 137, 1, 23-28. ISSN 0920-5861

Zha, Sh., Rauch, W., Liu, M., (2004), "Ni-$Ce_{0.9}Gd_{0.1}O_{1.95}$ Anode for GDC Electrolyte-Based Low-Temperature SOFCs", *Solid State Ionics*, 166, 3-4, 241–250. ISSN 0167-2738

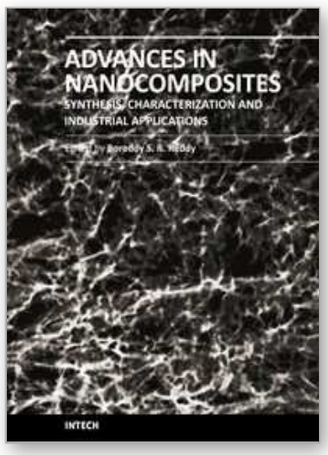

Advances in Nanocomposites - Synthesis, Characterization and Industrial Applications

Edited by Dr. Boreddy Reddy

ISBN 978-953-307-165-7
Hard cover, 966 pages
Publisher InTech
Published online 19, April, 2011
Published in print edition April, 2011

Advances in Nanocomposites - Synthesis, Characterization and Industrial Applications was conceived as a comprehensive reference volume on various aspects of functional nanocomposites for engineering technologies. The term functional nanocomposites signifies a wide area of polymer/material science and engineering, involving the design, synthesis and study of nanocomposites of increasing structural sophistication and complexity useful for a wide range of chemical, physicochemical and biological/biomedical processes. "Emerging technologies" are also broadly understood to include new technological developments, beginning at the forefront of conventional industrial practices and extending into anticipated and speculative industries of the future. The scope of the present book on nanocomposites and applications extends far beyond emerging technologies. This book presents 40 chapters organized in four parts systematically providing a wealth of new ideas in design, synthesis and study of sophisticated nanocomposite structures.

How to reference

In order to correctly reference this scholarly work, feel free to copy and paste the following:

Vladislav Sadykov, Natalia Mezentseva, Galina Alikina, Rimma Bunina, Vladimir Pelipenko, Anton Lukashevich, Zakhar Vostrikov, Vladimir Rogov, Tamara Krieger, Arkady Ishchenko, Vladimir Zaikovsky, Lyudmila Bobrova, Julian Ross, Oleg Smorygo, Alevtina Smirnova, Bert Rietveld and Frans van Berkel (2011). Nanocomposite Catalysts for Steam Reforming of Methane and Biofuels: Design and Performance, Advances in Nanocomposites - Synthesis, Characterization and Industrial Applications, Dr. Boreddy Reddy (Ed.), ISBN: 978-953-307-165-7, InTech, Available from: http://www.intechopen.com/books/advances-in-nanocomposites-synthesis-characterization-and-industrial-applications/nanocomposite-catalysts-for-steam-reforming-of-methane-and-biofuels-design-and-performance

INTECH
open science | open minds

InTech Europe
University Campus STeP Ri
Slavka Krautzeka 83/A
51000 Rijeka, Croatia
Phone: +385 (51) 770 447
Fax: +385 (51) 686 166
www.intechopen.com

InTech China
Unit 405, Office Block, Hotel Equatorial Shanghai
No.65, Yan An Road (West), Shanghai, 200040, China
中国上海市延安西路65号上海国际贵都大饭店办公楼405单元
Phone: +86-21-62489820
Fax: +86-21-62489821

IntechOpen